LsdD has a Critical Role in the Dehydrodiconiferyl Alcohol Catabolism among Eight Lignostilbene α,β-dioxygenase Isozymes in *Sphingobium* sp. Strain SYK-6

Naofumi Kamimura[a], Yusaku Hirose[a], Ryuto Masuba[a], Ryo Kato[a], Kenji Takahashi[a], Yudai Higuchi[a], Shojiro Hishiyama[b], and Eiji Masai[a*]

[a]Department of Bioengineering, Nagaoka University of Technology, Nagaoka, Niigata 940-2188, Japan

[b]Forestry and Forest Products Research Institute, Tsukuba, Ibaraki 305-8687, Japan

[*]For correspondence. Eiji Masai, Department of Bioengineering, Nagaoka University of Technology, Nagaoka, Niigata 940-2188, Japan. E-mail emasai@vos.nagaokaut.ac.jp; Tel. +81 258479428; Fax +81 258479450

Abstract

Lignin is the most abundant aromatic bioresource in nature, and elucidation of its biodegradation system is essential for understanding the carbon cycling on earth and its effective usage. The β−5 bond is one of the intermolecular linkages in lignin. *Sphingobium* sp. strain SYK-6 can assimilate various lignin-derived aromatic compounds, including a β−5 bond-containing dimer (phenylcoumaran-type), dehydrodiconiferyl alcohol (DCA). In the catabolic pathway of DCA, a stilbene-type compound, 3-(4-hydroxy-3-(4-hydroxy-3-methoxystyryl)-5-methoxyphenyl)acrylate (DCA-S), is produced. DCA-S is subjected to the cleavage of the interphenyl double bond by lignostilbene α,β-dioxygenase (LSD) to generate 5-formylferulate and vanillin. Among the eight LSD genes (*lsdA*–*lsdH*) found in the SYK-6 genome, the gene products of *lsdA*, *lsdC*, *lsdD*, and *lsdG* exhibited DCA-S conversion activity. The DCA-S conversion activity of SYK-6 was induced by vanillate produced as an intermediate metabolite of DCA-S. Of the LSD genes mentioned above, only the transcriptions of *lsdA*, *lsdD*, and *lsdG* were induced (2.6–10-fold) in the presence of vanillate. Analyses of *lsdA*, *lsdD*, and *lsdG* mutants showed that an *lsdD* mutant lost the DCA-S conversion activity under vanillate-induced conditions. These results demonstrate that *lsdD* plays a critical role in the converting DCA-S during the DCA catabolism in SYK-6.

Keywords

Lignin-derived dimers, Phenylcoumaran, Lignostilbene α,β-dioxygenase, Biodegradation, *Sphingobium* sp. SYK-6

1. Introduction

Lignin, a complex aromatic polymer, is a major component of the plant cell wall. Since lignin is the most abundant aromatic polymer on earth, its decomposition is essential for carbon recycling in nature, thus increasing its attention as a biorefinery resource. Lignin polymer is fundamentally composed of three *p*-hydroxyphenylpropanoid units known as canonical monolignols: coniferyl alcohol, sinapyl alcohol, and *p*-coumaryl alcohol (Vanholme et al., 2019). Random coupling of these monolignols makes a lignin polymer. In lignin, phenylpropane units derived from monolignols are connected via C–C and C–O–C bonds (Ralph et al., 2019; Vanholme et al., 2010). The most predominant linkage is β–O–4 (β-aryl ether) but lignin has the β–5 (phenylcoumaran), 5–5 (biphenyl), β–β (pinoresinol), and β–1 (diarylpropane) linkages. In nature, lignin is biologically degraded via two main stages as follows: depolymerization of native lignin by white-rot fungi (Floudas et al., 2012; Martínez et al., 2018; Martínez et al., 2009) and catabolism of resultant heterogeneous low-molecular-weight aromatic compounds by bacteria (Bugg et al., 2011; Kamimura et al., 2019; Kamimura et al., 2017b; Masai et al., 2007; Ralph et al., 2019). Therefore, elucidation of bacterial catabolism for lignin-derived aromatic compounds is essential for understanding the final stage of lignin biodegradation in nature.

In bacteria, lignin-derived dimers and monomers are catabolized through convergent pathways. These processes called “biological funneling” are getting much attention as a promising bioconversion tool for developing technology to produce value-added bioproducts from heterogeneous low-molecular-weight aromatic compounds obtained by chemo-catalytic depolymerization of lignin (Becker and Wittmann, 2019; Beckham et al., 2016; Shinoda et al., 2019; Sonoki et al., 2017). A considerable amount of knowledge regarding bacterial catabolism of lignin-derived monomers has been gathered (Bugg et al., 2011; Kamimura et al., 2017b; Masai et al., 2007); however, enzymes and enzyme genes responsible for dimer catabolism have not been fully identified.

Sphingobium sp. strain SYK-6, an alphaproteobacterium, is the best-characterized bacterium for the catabolism of lignin-derived aromatic compounds (Higuchi et al., 2017; Kamimura et al., 2017b; Masai et al., 2007). SYK-6 assimilates various lignin-derived dimers, including β-aryl ether, biphenyl, phenylcoumaran, and diarylpropane, as well as monomers, including ferulate, vanillin, and vanillate. This study focused on the catabolism of a phenylcoumaran-type dimer in SYK-6. The β–5 bond that forms the phenylcoumaran structure makes up approximately 3%–10% of the total intermolecular linkages in lignin. A phenylcoumaran-type dimer, dehydrodiconiferyl alcohol (DCA), is a significant dilignol generated during the early stage of plant lignin formation (Davin et al., 1997; Lewis et al.,

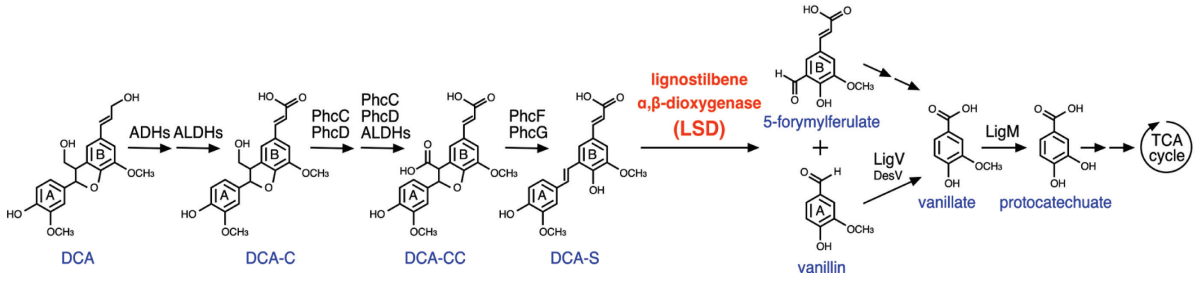

Fig. 1. Catabolic pathway of dehydrodiconiferyl alcohol in *Sphingobium* sp. strain SYK-6. Enzymes: ADHs, alcohol dehydrogenases; ALDHs, aldehyde dehydrogenases; PhcC and PhcD, enantiospecific DCA-C oxidases; PhcF and PhcG, enantiospecific DCA-CC decarboxylases; LSD, Lignostilbene α,β-dioxygenase; LigV, vanillin dehydrogenase; DesV, syringaldehyde dehydrogenase; LigM, vanillate/3-*O*-methylgallate *O*-demethylase. Compounds: DCA, dehydrodiconiferyl alcohol; DCA-C, 3-(2-(4-hydroxy-3-methoxyphenyl)-3-(hydroxymethyl)-7-methoxy-2,3-dihydrobenzofuran-5-yl)acrylate; DCA-CC, 5-(2-carboxyvinyl)-2-(4-hydroxy-3-methoxyphenyl)-7-methoxy-2,3-dihydrobenzofuran-3-carboxylate; DCA-S, 3-(4-hydroxy-3-(4-hydroxy-3-methoxystyryl)-5-methoxyphenyl)acrylate.

1998). An overview of the DCA catabolic pathway was determined in *Sphingomonas paucimobilis* TMY1009 (Habu et al., 1988) and has recently been detailed in SYK-6 (Takahashi et al., 2015; Takahashi et al., 2014; Takahashi et al., 2018) (Fig. 1). In SYK-6, the alcohol group of the DCA B-ring side chain is subjected to continuous oxidation by multiple alcohol and aldehyde dehydrogenases to produce 3-(2-(4-hydroxy-3-methoxyphenyl)-3-(hydroxymethyl)-7-methoxy-2,3-dihydrobenzofuran-5-yl)acrylate (DCA-C). Glucose-methanol-choline oxidoreductase family enzymes, PhcC and PhcD, oxidize the alcohol group of the DCA-C A-ring side chain to produce 5-(2-carboxyvinyl)-2-(4-hydroxy-3-methoxyphenyl)-7-methoxy-2,3-dihydrobenzofuran-3-carboxylate (DCA-CC) via an aldehyde derivative. The resultant DCA-CC is decarboxylated by DUF3237 domain-containing enzymes, PhcF and PhcG, to form a stilbene compound, 3-(4-hydroxy-3-(4-hydroxy-3-methoxystyryl)-5-methoxyphenyl)acrylate (DCA-S). The DCA-C oxidation by PhcC/PhcD and the DCA-CC decarboxylation by PhcF/PhcG are catalyzed in an enantiospecific manner (Takahashi et al., 2015; Takahashi et al., 2018). DCA-S is subjected to the cleavage of the interphenyl Cα–Cβ double bond of the A-ring side chain to generate 5-formylferulate and vanillin.

It has been suggested that lignostilbene α,β-dioxygenase (LSD) is involved in converting DCA-S in *S. paucimobilis* TMY1009 (Habu et al., 1989b). LSDs belong to the carotenoid cleavage oxygenase (CCO) family and catalyze the cleavage of the interphenyl Cα–Cβ double bond of 4-[(1*E*)-2-(4-hydroxy-3-methoxyphenyl)ethenyl]-2-methoxyphenol (HMPPD-S) via the incorporation of two oxygen atoms; therefore, generating two molecules of vanillin (Daruwalla and Kiser, 2020; Kamoda et al., 1989; Poliakov et al., 2020). TMY1009 has four

LSD isozymes, which are active against DCA-S to varying degrees, Lsd-I [homodimer of LsdA(α)$_{TMY}$, accession no, AAC60447.2], Lsd-II [homodimer of LsdB(β)$_{TMY}$, AAB35856.2], LSD-III (heterodimer of LsdA$_{TMY}$ and LsdB$_{TMY}$), and LSD-IV (homodimer of Lsdγ, PC4390) (Kamoda and Saburi, 1993; Kamoda et al., 1997, 2005). Recently, Kuatsjah et al. performed biochemical and structural analysis of LsdA$_{TMY}$ and showed catalytic parameters, substrate specificity, and catalytic mechanisms (Kuatsjah et al., 2019). LsdA$_{TMY}$ is highly specific for HMPPD-S, which has been suggested to be an intermediate metabolite of the β−1 model dimer, 1,2-bis(4-hydroxy-3-methoxyphenyl)-1,3-propanediol (HMPPD) (Habu et al., 1989a). However, the actual LSD gene(s) responsible for converting DCA-S in DCA catabolism in vivo has not been identified in any bacteria.

Here, of eight LSD isozyme genes in the SYK-6 genome, we searched for the LSD gene(s) responsible for DCA-S conversion in DCA catabolism. The genes were narrowed down from the eight candidates based on transcript levels and inducibility and the DCA-S conversion activity of each purified LSD. Finally, analysis of the gene-disrupted mutants identified the LSD gene involved in DCA-S catabolism in SYK-6.

2. Materials and methods

2.1. Bacterial strains, plasmids, and culture conditions

The strains and plasmids used in this study are listed in Table S1. *Sphingobium* sp. strain SYK-6 (NBRC 103272/JCM 17495) and its mutants were grown in lysogeny broth (LB) or Wx minimal medium supplemented with 10 mM sucrose, 10 mM glutamate, 10 mM proline, and 0.34 mM methionine (Wx-SEMP) (Araki et al., 2020), Wx-SEMP supplemented with 2 mM DCA, 5 mM vanillate, or 5 mM protocatechuate at 30°C with shaking (160 rpm). *Sphingobium japonicum* UT26S and *Pseudomonas putida* PpY1100 were grown in LB at 30°C with shaking. When necessary, 50 mg kanamycin liter^{-1}, 100 mg streptomycin liter^{-1}, 12.5 mg tetracycline liter^{-1}, or 300 mg carbenicillin liter^{-1} were added to the cultures. *Escherichia coli* strains were grown in LB at 37°C. Media for *E. coli* transformants carrying antibiotic resistance markers were supplemented with 100 mg ampicillin liter^{-1} or 25 mg kanamycin liter^{-1}.

2.2. Preparation of chemicals

DCA, DCA-S, and 5-formylferulate were prepared as described previously (Takahashi et al., 2014; Takahashi et al., 2018). Vanillate, protocatechuate, 4-hydroxystilbene, isorhapontigenin, resveratrol, pinostilbene, piceatannol, isoeugenol, 3,4',5-trimethoxy-stilbene, dehydrozingerone, and 3-hexenedioate were purchased from Tokyo Chemical Industry Co., Ltd (Tokyo, Japan). HMPPD-S was synthesized as shown in the supplemental material.

2.3. DNA manipulations and sequence analysis

Primers used in this study are listed in Table S2. DNA sequences were determined by Eurofins Genomics (Tokyo, Japan). Sequence analysis was performed using the MacVector program version 17.5.2 (NC, USA). Sequence similarity searches, multiple alignments, and pairwise alignments were performed using the BLAST (basic local alignment search tool) program (Johnson et al., 2008), Clustal Omega program (Sievers et al., 2011), and the EMBOSS Needle program (Madeira et al., 2019), respectively. A phylogenetic tree was generated using the MEGA X program (Kumar et al., 2018).

2.4. Expressions of lsdA–lsdH in heterologous hosts and enzyme purification

DNA fragments carrying each *lsd* gene with the NdeI site at 5' terminus and the BamHI/XhoI site at 3' terminus were amplified by PCR from the SYK-6 total DNA. The amplified fragments digested with NdeI and BamHI/XhoI were cloned into corresponding

sites of pET-16b. For expression of *lsdE* in *S. japonicum* UT26S, a 1.5-kb fragment carrying *lsdE* with a 6× His-tag sequence at the 5' terminus was amplified from the SYK-6 total DNA, and then the resulting fragment was cloned into the HindIII site of pQF using an NEBuilder HiFi DNA assembly cloning kit (New England Biolabs, MA, USA) to generate pQFlsdE. Nucleotide sequences of the resultant plasmids were then confirmed. For expression of *lsdH* in *P. putida* PpY1100, a 1.6-kb XbaI-BamHI fragment carrying *lsdH* was cloned from pET37540 into the same sites of pBluescript II KS(+) to generate pBKS37540H. A 1.6-kb NotI-BamHI fragment carrying *lsdH* from pBKS37540H was cloned into the same sites of pJB864 to generate pJB37540. Introduction of plasmids into *S. japonicum* and *P. putida* was performed by electroporation. Cells of *E. coli* BL21(DE3) harboring pET09440, pET11300, pET12580, pET12860, pET27300, pET27970, pET36640, or pET37540 were grown in LB at 30°C. Each gene expression was induced for 4 h at 30°C by adding 1 mM isopropyl-β-D-galactopyranoside when the optical density at 600 nm (OD_{600}) of the culture reached 0.5. Cells of *S. japonicum* harboring pQFlsdE were inoculated into LB supplemented with 0.1 mM cumate as an inducer and grown at 30°C for 16 h. Cells of *P. putida* harboring pJB37540 were inoculated into LB supplemented with 1 mM *m*-toluate as an inducer and grown at 30°C for 12 h. The resultant cultures of *E. coli*, *S. japonicum*, and *P. putida* transformants were then harvested by centrifugation at 7,000 × *g* for 5 min at 4°C. Cells were washed twice with 50 mM Tris-HCl (pH 7.5; buffer A) and resuspended in the same buffer. The cells were then disrupted using an ultrasonic disintegrator. After centrifugation (19,000 × *g* for 15 min at 4°C), the supernatants were obtained as cell extracts.

For purification of LsdA–LsdH, cell extracts of *E. coli* harboring pET09440, pET11300, pET12580, pET12860, pET27970, and pET36640; *S. japonicum* harboring pQFlsdE; and *P. putida* harboring pJB37540, were transferred onto a His SpinTrap column (GE Healthcare, WI, USA). Purification of His-tag fused proteins was performed according to the instruction manual. Resultant elution fractions were subjected to desalting and concentration using an Amicon Ultra centrifugal filter unit (30 kDa cutoff; Merck Millipore, MA, USA). The preparation of cell extracts and purification processes were performed under aerobic conditions. Gene expressions and the preparations' purity were examined by sodium dodecyl sulfate-polyacrylamide gel electrophoresis (SDS-PAGE) using 12% polyacrylamide gel. The protein bands in gels were stained with Coomassie Brilliant Blue. Protein concentrations were determined using the Bradford method with bovine serum albumin as the standard (Bio-Rad, CA, USA).

2.5. Identification of reaction products

Purified enzymes (20 μg of protein ml^{-1}) were incubated with 100 μM DCA-S, HMPPD-S, 4-hydroxystilbene, isorhapontigenin, resveratrol, pinostilbene, piceatannol, isoeugenol, 3,4',5-trimethoxy-stilbene, dehydrozingerone, and 3-hexenedioate in buffer A for 10 min (DCA-S and HMPPD-S) or 30 min (other substrates) at 30°C. The reactions were stopped by adding acetonitrile to a final concentration of 50%. Precipitated proteins were removed by centrifugation at 19,000 × *g* for 15 min at 4°C. The resulting supernatant diluted with 50% acetonitrile (final concentration, 25%) was filtered and analyzed by a high-performance liquid chromatography (HPLC) and HPLC–mass spectrometry (HPLC–MS) analysis using the Acquity ultraperformance liquid chromatography (UPLC) system (Waters, MA, USA) coupled with an Acquity TQ detector (Waters) using a TSKgel ODS-140HTP column (2.1 × 100 mm; Tosoh, Tokyo, Japan) as previously described (Fukuhara et al., 2010). The mobile phase of the HPLC system was a mixture of water (75%) and acetonitrile (25%) containing formate (0.1%) at a flow rate of 0.5 ml min^{-1}. DCA-S and HMPPD-S were detected at 326 nm. Other compounds were detected at 300 nm. Retention times: DCA-S, 4.3 min; HMPPD-S, 5.1 min; 4-hydroxystilbene, 4.5 min; isorhapontigenin, 2.8 min; resveratrol, 2.8 min; pinostilbene, 3.6 min; piceatannol, 2.2 min; and isoeugenol, 3.8 min.

2.6. Enzyme assay for purified LSD

According to the instruction manual, enzyme activities of purified enzymes were determined by monitoring molecular oxygen consumption using an Oxygraph PLUS System (Hansatech Instruments Ltd., Norfolk, UK). Purified enzymes (20 μg of protein ml^{-1}) were incubated with buffer A in a chamber at 30°C. The reaction was initiated by adding 100 μM substrates (reaction volume, 500 μl). The electrode was calibrated before the reaction using air-saturated water and O_2-depleted water prepared using sodium hydrosulfite. The specific activity of DCA-S conversion was calculated from the rate of O_2 consumption.

2.7. Enzyme assay for SYK-6 cell extracts

Cells of SYK-6 and its mutants grown in LB were washed twice with Wx buffer [12.5 mM KH_2PO_4, 27.4 mM Na_2HPO_4, and 7.6 mM $(NH_4)_2SO_4$ (pH 7.1)], suspended in the same buffer and inoculated into Wx-SEMP to an OD_{600} of 0.2. After that, the cells were cultured until the OD_{600} reached 0.5, 2 mM DCA, 5 mM vanillate, or 5 mM protocatechuate was added to the cultures, and then the cells were further incubated for 2 or 6 h. For the analysis of transformants of SYK-6 and its mutants, cells were inoculated into Wx-SEMP supplemented with 0.1 mM cumate as an inducer and grown for 16 h. The cell extracts were prepared as described above and used for DCA-S conversion assays. Cell extracts (10–100 μg of protein ml^{-1}) were

incubated with 100 μM DCA-S in buffer A at 30°C for 5 min. The reactions were stopped by adding acetonitrile, and the concentrations of DCA-S were analyzed by HPLC. Specific activities for DCA-S conversion by cell extracts were expressed in moles of converted DCA-S per min per milligram of protein.

2.8. Quantitative reverse transcription-PCR (qRT-PCR) analysis

SYK-6 cells were grown in Wx-SEMP or Wx-SEMP supplemented with 2 mM DCA, 5 mM vanillate, or 5 mM protocatechuate as described above. Total RNA was isolated from resultant cells as described previously (Araki et al., 2019). cDNAs were synthesized by reverse transcription using random hexamer and SuperScript IV reverse transcriptase (Invitrogen, MA, USA) from total RNA (2 μg). The synthesized cDNA was purified using a NucleoSpin Gel and PCR Clean-up Kit (Takara Bio, Shiga, Japan). Quantitative PCR reactions were performed using purified cDNA sample, primers (Table S3), and FAST SYBR green PCR master mix (Applied Biosystems, MA, USA) in a Step One real-time PCR system (Applied Biosystems) according to the instruction manual. Primer pairs were designed using Primer Express software version 3.0 (Applied Biosystems). The amounts of each mRNA and 16S rRNA were measured using standard DNAs. To normalize the amount of mRNA in each sample, 16S rRNA was used as an internal standard.

2.9. Construction of mutants

Mutants with deletion of *lsdA*, *lsdC*, *lsdD*, and *lsdG* in SYK-6 were constructed by homologous recombination. DNA fragments carrying upstream and downstream regions (approx. 1.0 kb each) of each gene were amplified by PCR from SYK-6 total DNA. The resultant fragments were cloned into pAK405 (Kaczmarczyk et al., 2012) by an In-Fusion HD cloning kit (Takara Bio) or an NEBuilder HiFi DNA assembly cloning kit. Each resulting plasmid was introduced into SYK-6 cells by triparental mating, and the mutants were selected as described previously (Kaczmarczyk et al., 2012). Gene deletion was confirmed by colony PCR. For complementation of the *lsdD* mutant (Δ*lsdD*), a DNA fragment carrying *lsdD* was amplified from SYK-6 total DNA using primers (Table S3) and cloned into the Hind III site of pQF by an NEBuilder HiFi DNA assembly cloning kit to generate pQFlsdD. Each pQF and pQFlsdD was introduced into SYK-6 and Δ*lsdD* cells by electroporation, and the resulting transformants were used for the DCA-S conversion assay.

2.10. Statistical analysis

All results were obtained from n = 3 independent experiments. Statistical tests were

performed by unpaired, two-tailed Student's *t*-test using GraphPad Prism software version 8 (GraphPad Software, CA, USA). $P < 0.05$ was considered statistically significant.

3. Results

3.1. Search for LSD-like enzyme genes in Sphingobium sp. strain SYK-6

A BLAST search of the SYK-6 genome using amino acid sequences of $LsdA_{TMY}$ (AAC60447.2) of *S. paucimobilis* TMY1009, $LsdB_{TMY}$ (AAB35856.2) of TMY1009, and NOV1 (ABD25247.1) of *Novosphingobium aromaticivorans* DSM 12444 as queries revealed eight genes (SLG_12580 [previously named *lsdA*], SLG_09440 [*lsdB*], SLG_11300 [*lsdC*], SLG_12860 [*lsdD*], SLG_27300 [*lsdE*], SLG_27970 [*lsdF*], SLG_36640 [*lsdG*], and SLG_37540[*lsdH*]) exhibiting 35%–99% amino acid sequence identities with $LsdA_{TMY}$, $LsdB_{TMY}$, or NOV1. LsdH, LsdG, and LsdD showed the highest similarity with $LsdA_{TMY}$ (99% identity), $LsdB_{TMY}$ (98% identity), and NOV1 (79% identity), respectively (Table S3). Also, N-terminal amino acid sequence of LsdD (25 amino acids) is completely consistent with that of Lsdγ of TMY1009 (PC4390) (Kamoda et al., 1997). Phylogenetic analysis of SYK-6 LsdA–LsdH with previously characterized LSDs, resveratrol cleavage oxygenases (RCOs), isoeugenol monooxygenases (IEMs), carotenoid cleavage oxygenases (CCOs), and carotenoid isomerooxygenases showed that these enzymes were separated into three clades: LSD/RCO/IEM, CCO, and carotenoid isomerooxygenase (Fig. S1). LsdA–LsdH are all included in the LSD/RCO/IEM clade (Fig. S1). In the LSD/RCO/IEM clade, LsdC, LsdD, LsdG, and LsdH formed a subclade together with $LsdA_{TMY}$, $LsdB_{TMY}$, and NOV1. In contrast, LsdA, LsdB, and LsdF created a subclade with NOV2, whereas LsdE was relatively close to a subclade, including RCOs and IEMs (Fig. S1 and Table S1). Recent structural analyses of NOV1 and $LsdA_{TMY}$ revealed that four histidines (His167, His218, His284, and His476 in NOV1) coordinate an iron cofactor, and $Tyr101_{NOV1}$ and $Lys135_{NOV1}$ stimulate the deprotonation of the 4-OH group of substrates critical for catalyzing Cα–Cβ cleavage (Kuatsjah et al., 2019; Marasco and Schmidt-Dannert, 2008). An alignment of LsdA–LsdH with previously characterized LSDs showed that all of these four His, Tyr, and Lys are conserved in LsdA–LsdH (Fig. S2).

3.2. Characterization of the SYK-6 lsd gene products

To examine the catalytic ability of LsdA–LsdH, the *lsdA–lsdH* genes were expressed in heterologous hosts. *lsdA*, *lsdB*, *lsdC*, *lsdD*, and *lsdG* were cloned into pET-16b, and His-tag fused proteins were produced in *E. coli* (Fig. S3A). Since LsdE and LsdH were scarcely produced in *E. coli* transformants, His-tag fused *lsdE* and *lsdH* were cloned into pQF and pJB864 and expressed in *Sphingobium japonicum* UT26S and *Pseudomonas putida* PpY1100, respectively (Fig. S3A). LsdA–LsdH were purified to near homogeneity by Ni affinity chromatography under aerobic conditions (Fig. S3B).

Activities of LsdA–LsdH toward twelve substrates, including stilbene derivatives, such as intermediate metabolites of DCA (DCA-S) and HMPPD (HMPPD-S), were evaluated using an oxygen consumption assay (Fig. 2 and S4). The reaction products were analyzed by HPLC–MS to verify whether LsdA–LsdH catalyze the cleavage of the C–C double bond of each substrate (Fig. S5). LsdA–LsdH were active to varying degrees against any lignostilbene derivatives, suggesting that these enzymes are indeed LSD. LsdA exhibited the broadest substrate range, converting DCA-S, HMPPD-S, 4-hydroxystilbene, isorhapontigenin, resveratrol, pinostilbene, piceatannol, and isoeugenol (Fig. 2). LsdA–LsdH other than LsdE converted more than four tested substrates, whereas LsdE converted only HMPPD-S and piceatannol with low activity (<0.2 μmol min^{-1} mg^{-1}). Although all LSD isozymes showed activity toward HMPPD-S, DCA-S conversion capacity was observed only in LsdA, LsdC,

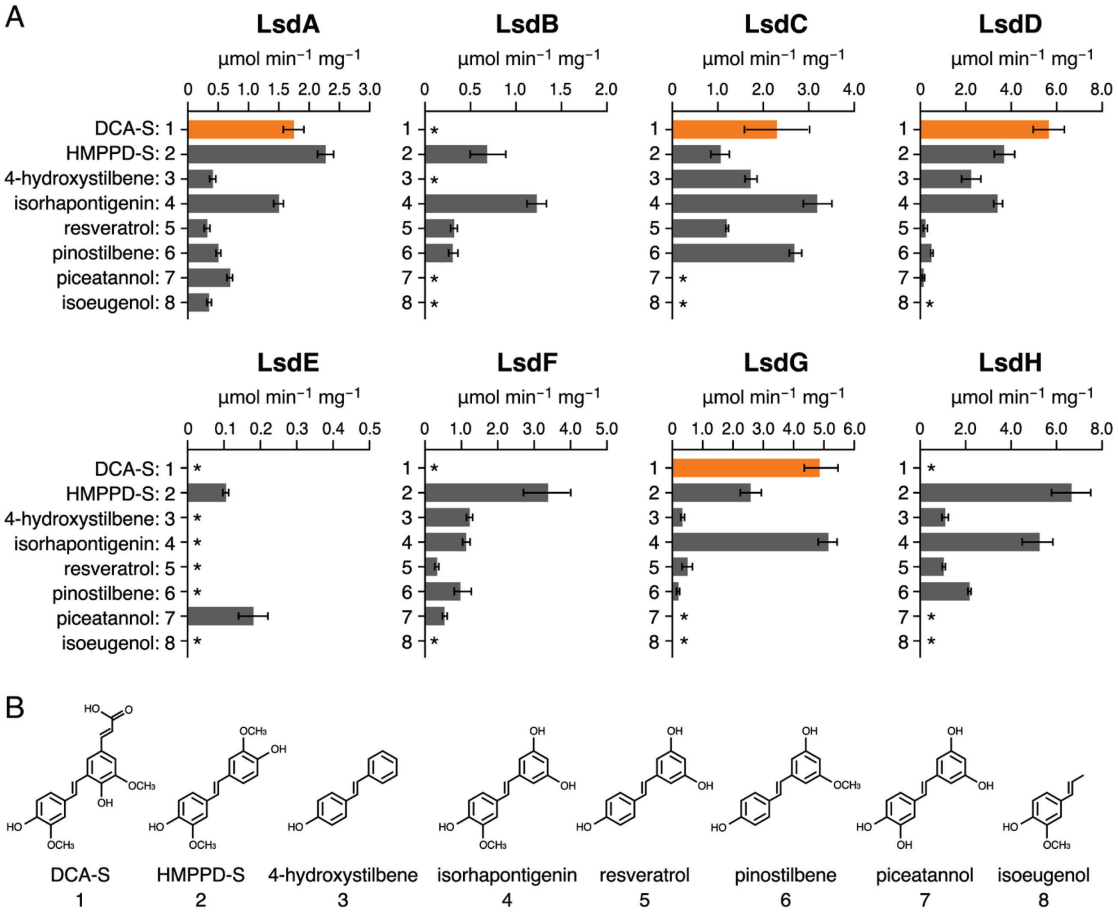

Fig. 2. Substrate range of LsdA–LsdH. (A) Purified enzymes (20 μg of protein ml^{-1}) were incubated with 100 μM substrates shown in panel B. Specific activities of substrate conversion were calculated from the amount of molecular oxygen consumed. All experiments were performed in triplicate, and each value represents the mean ± standard deviation. Asterisks indicate activities lower than 0.05 μmol min^{-1} mg^{-1}. (B) Chemical structure of substrates.

LsdD, and LsdG. LsdD and LsdH showed the highest activity toward DCA-S (5.4 ± 0.7 μmol min^{-1} mg^{-1}) and HMPPD-S (6.6 ± 0.9 μmol min^{-1} mg^{-1}), respectively. Among the substrates examined, LsdA–LsdH showed the highest activity toward DCA-S, HMPPD-S, or isorhapontigenin, suggesting their preference for 4-hydroxy-3-methoxystilbenes. No Lsd enzyme converted 3,4',5-trimethoxy-stilbene, dehydrozingerone, and 3-hexenedioate.

3.3. Induction profile of SYK-6 DCA-S conversion and lsd gene expression

To examine whether the conversion of DCA-S by SYK-6 is inducible or not, the rates of 100 μM DCA-S conversion were measured using extracts of SYK-6 cells grown in Wx-SEMP supplemented with and without 2 mM DCA. The conversion rate of the extract from cells grown with 2 mM DCA was 2.1-fold (induction for 2 h) and 8.2-fold (induction for 6 h) higher than that of the extract from the cells grown without DCA (Fig. 3A). These results suggest that inducible enzymes are involved in the conversion of DCA-S during the DCA catabolism. To identify the inducer, we examined the inducibility of DCA-S conversion by a double mutant of *phcC* and *phcD* (SME112, Δ*phcCD*), which cannot convert DCA-C (Fig. 1). The DCA-S conversion rate was not promoted in Δ*phcCD* cells after 2 and 6 h incubation with 2 mM DCA, suggesting that the inducer is a metabolite generated from DCA-C (Fig.

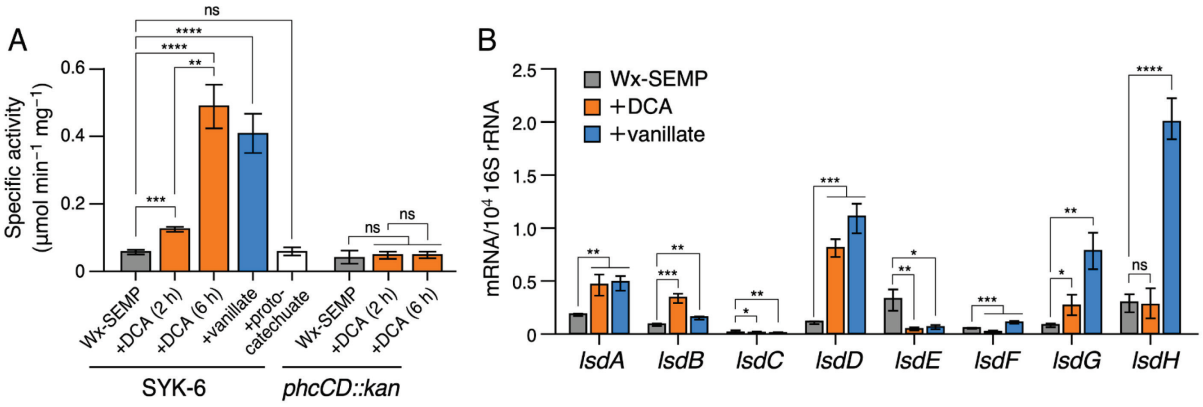

Fig. 3. Induction profiles of SYK-6 DCA-S conversion and *lsd* gene expression. (A) Induction of DCA-S conversion activity. Cells of SYK-6 and Δ*phcCD* were grown in Wx-SEMP (gray), Wx-SEMP + 2 mM DCA (orange), Wx-SEMP + 5 mM vanillate (blue), and Wx-SEMP + 5 mM protocatechuate (white). Extracts of resultant cells (10–100 μg protein ml^{-1}) were incubated with 100 μM DCA-S at 30°C for 5 min, and specific activities for DCA-S conversion were measured. Parentheses show the induction time with DCA. (B) qRT-PCR analyses of the transcription of *lsd* genes. Total RNA was isolated from SYK-6 cells grown in Wx-SEMP (gray), Wx-SEMP + 2 mM DCA (orange), and Wx-SEMP + 5 mM vanillate (blue). Values for each mRNA level were normalized to 16S rRNA. All experiments were performed in triplicate, and each value represents the mean ± standard deviation. Statistical differences were determined by Student's *t*-test. The asterisks indicate statistically significant differences between the values linked by brackets (ns, $P > 0.05$; *, $P < 0.05$; **, $P < 0.01$; ***, $P < 0.001$; ****, $P < 0.0001$).

3A). Next, the inducibility of DCA-S conversion by SYK-6 was evaluated using the cells grown with vanillate or protocatechuate, metabolites of DCA-C. When the SYK-6 cells were incubated in Wx-SEMP plus 5 mM vanillate for 6 h, the DCA-S conversion rate increased to the same level as 6 h of DCA induction (Fig. 3A). Such induction of activity was not observed in the cells grown in the presence of protocatechuate. These results strongly suggest that vanillate is an inducer of the *lsd* gene involved in DCA-S conversion during DCA catabolism in SYK-6.

Based on the results of our previous DNA microarray analysis (Fujita et al., 2019), we examined the transcriptional induction profiles of *lsdA–lsdH* and DCA catabolism genes (*phcC*, *phcD*, *phcF*, and *phcG*) in SYK-6 cells grown in Wx-SEMP supplemented with and without 2 mM DCA, 5 mM vanillate, or 5 mM protocatechuate. Among *lsdA–lsdH*, transcription of *lsdD* increased 4.2-fold during growth with DCA, along with a 2.2–6.1-fold increase in transcriptions of *phcC*, *phcD*, *phcF*, and *phcG* (Table S4). Besides, *lsdA*, *lsdD*, and *lsdH* were induced more than 2-fold during growth with vanillate. In contrast, there was no induction of any genes in the cells grown in the presence of protocatechuate (induction ratio < 2.0). To verify these induction profiles, qRT-PCR analyses of *lsdA–lsdH* were performed using cells grown in Wx-SEMP supplemented with and without 2 mM DCA or 5 mM vanillate (Fig. 3B). Transcription levels of *lsdA*, *lsdB*, *lsdD*, and *lsdG* were increased by 1.7–10.4-fold under DCA- and vanillate-induced conditions compared to uninduced conditions. Under DCA-induced conditions, *lsdD* showed the highest transcription level. *lsdH* was not induced under DCA-induced conditions but showed the highest transcription level among *lsd* genes under vanillate-induced conditions. Among the LSD isozymes that converted DCA-S (LsdA, LsdC, LsdD, and LsdG), the transcription levels of *lsdC* under DCA- and vanillate-induced conditions were 31–100 times lower than those of *lsdA*, *lsdD*, and *lsdG*, suggesting the small contribution of *lsdC* to the DCA-S conversion.

3.4. Role of LSD isozymes in DCA catabolism

Based on the transcription profiles of *lsdA–lsdH* and DCA-S conversion capacity of their gene products, *lsdA*, *lsdD*, and *lsdG* appeared to play a significant role in the DCA-S conversion during DCA catabolism. Deletion mutants of *lsdA* (Δ*lsdA*), *lsdD* (Δ*lsdD*), and *lsdG* (Δ*lsdG*) were created by homologous recombination (Fig. S6), and their DCA-S conversion activities were evaluated using cell extracts. Since transcriptions of *lsdA*, *lsdD*, and *lsdG* were induced under vanillate-induced conditions, cell extracts were prepared from the cells grown in Wx-SEMP supplemented with and without 5 mM vanillate. Both under vanillate-induced and uninduced conditions, Δ*lsdD* lost the DCA-S conversion activity (Fig.

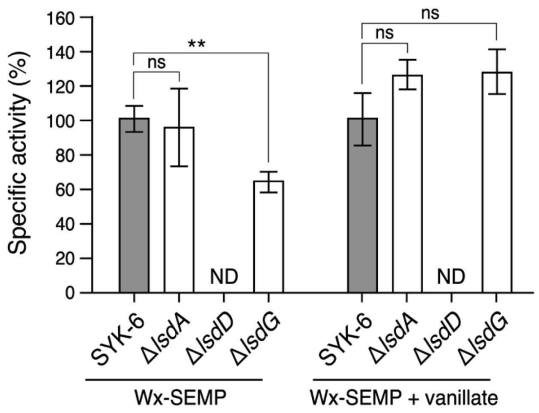

Fig. 4. DCA-S conversion capacity of mutants of *lsdA*, *lsdD*, and *lsdG*. Cells of SYK-6, Δ*lsdA*, Δ*lsdD*, and Δ*lsdG* were grown in Wx-SEMP or Wx-SEMP + 5 mM vanillate. Extracts of resultant cells (10–100 μg protein ml^{-1}) were incubated with 100 μM DCA-S at 30°C for 5 min, and specific activities for DCA-S conversion were measured. Each value represents the relative activity when the values of SYK-6 (Wx-SEMP, 0.060 ± 0.004 μmol min^{-1} mg^{-1}; Wx-SEMP + vanillate, 0.41 ± 0.06 μmol min^{-1} mg^{-1}) were set to 100%. ND, not detected. Statistical differences were determined by Student's *t*-test. The asterisks indicate statistically significant differences between the values linked by brackets (ns, $P > 0.05$; **, $P < 0.01$).

4). In contrast, Δ*lsdG* showed a 37% reduction in activity (0.039 ± 0.003 μmol min^{-1} mg^{-1}) than the wild type (0.060 ± 0.004 μmol min^{-1} mg^{-1}) when cells were cultured under uninduced conditions. To verify whether the disruption of *lsdD* caused DCA-S conversion deficiency by Δ*lsdD*, we examined the conversion activity of Δ*lsdD* harboring pQFlsdD carrying *lsdD*. Δ*lsdD*(pQFlsdD) showed a significantly high DCA-S conversion activity (6.2 ± 0.8 μmol min^{-1} mg^{-1}) similar to SYK-6(pQFlsdD) (5.1 ± 0.4 μmol min^{-1} mg^{-1}). These results indicate that *lsdD* plays a critical role in DCA-S conversion by SYK-6 during DCA catabolism.

4. Discussion

This study identified the LSD gene responsible for the conversion of DCA-S in SYK-6. Among the eight LSD isozyme genes, we revealed that *lsdD*, whose transcription is induced during DCA catabolism, plays a crucial role in DCA-S conversion. The analysis of the induction profile strongly suggested that vanillate is an inducer for the transcription of *lsdD*. During DCA catabolism, vanillate is generated from vanillin and 5-formylferulate, both produced by the double-bond cleavage of DCA-S (Fig. 5). Therefore, the transcription of *lsdD* is induced via the feedback action of vanillate. The conversion of DCA-S during DCA catabolism is considered to proceed as follows (Fig. 5). First, DCA-S is converted by a small amount of LsdD producing vanillin and 5-formylferulate. Vanillin is subsequently converted to vanillate by the gene products of constitutively expressing *ligV* and *desV* (Kamimura et al., 2017a). Besides, 5-formylferulate is also converted to vanillate. The resulting vanillate triggers the activation of DCA-S conversion through the induction of *lsdD*, and this activation appears to continue until DCA is depleted.

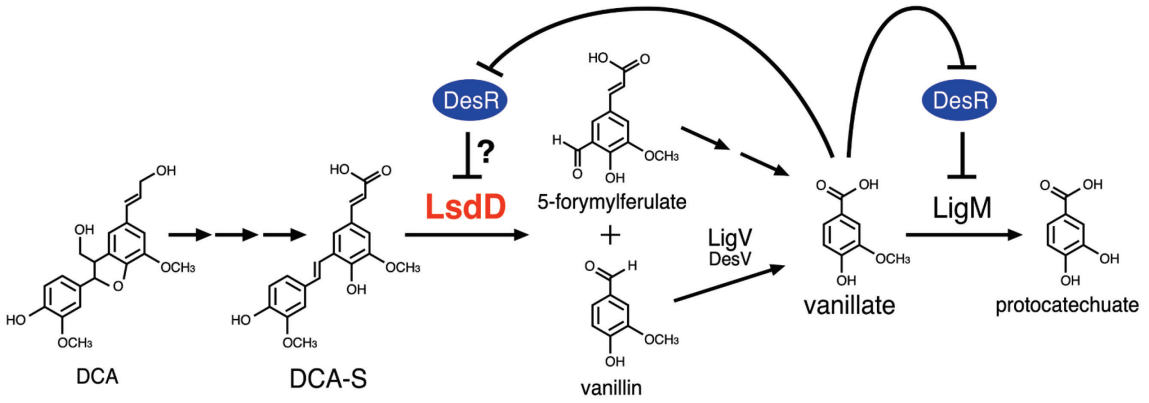

Fig. 5. Proposed regulation of the DCA-S catabolism in SYK-6. DCA-S is converted by the gene product of *lsdD*, whose transcription is induced via the feedback action of vanillate. Transcription of *lsdD* is considered negatively regulated along with *ligM* by DesR, which uses vanillate as an effector molecule.

In SYK-6, two types of transcriptional regulatory systems that use vanillate as the inducer have been clarified: i) negative regulation by a MarR-type repressor (DesR) of vanillate/3-*O*-methyl gallate *O*-demethylase gene (*ligM*), gallate dioxygenase gene (*desB*), and *desR* (Araki et al., 2019); ii) negative regulation of syringate *O*-demethylase gene (*desA*) by an IclR-type repressor (DesX) (Araki et al., 2020; Araki et al., 2019). DesR binds to the inverted repeat (IR) sequences, IR-M (5′-GTTTGTGTAACATAC-3′), IR-B (5′-GTTTGTGTCACATAC-3′), and IR-R (5′-GTATGCTACGCTTAC-3′), which are located upstream of *ligM*, *desB*, and *desR*, respectively (Fig. S7A–C) (Araki et al., 2019). In contrast, DesX binds to IR-DA (5′-

TCTTCGTATATACGAAGA-3′) located upstream of SLG_25010 that consists of an operon with *desA* (Fig. S7D). *lsdD* is located directly upstream of *desR* and both genes have different transcriptional directions (Fig. S7C). IR-R locates at positions −39 to −25 from the start codon of *lsdD*. Considering the position of IR-R and the fact that *lsdD* is induced by vanillate, it is likely that binding of DesR to IR-R represses not only *desR* but also *lsdD* transcription at the same time (Fig. 5). In addition to *lsdD*, transcription levels of *lsdG* and *lsdH* were also strongly increased under vanillate-induced conditions (Fig. 3B). Since neighboring SLG_36630 and *lsdG* (SLG_36640) as well as neighboring *lsdH* (SLG_37540) and SLG_37550 have different transcriptional directions, respectively (Fig. S8), there exist a promoter region in each intergenic region. A search for possible regulatory motifs in these intergenic regions revealed incomplete IR sequences distinct from the binding sequences of DesR and DesX (Fig. S8). Unidentified regulators that recognize these IR sequences may be involved in the induction of *lsdG* and *lsdH* in cells cultured with vanillate.

Around *lsdD*, there are protocatechuate transporter gene (*pcaK*) (Mori et al., 2018), β-hydroxypropiovanillone oxidase gene (*hpvZ*) (Higuchi et al., 2018), and 5-carboxyvanillate decarboxylase gene (*ligW2*) (Peng et al., 2005) in addition to *desR*. Similar to the gene organization around *lsdD* in SYK-6, homologous genes of *desR* (Saro_0803), *pcaK* (Saro_0804), and *ligW2* (Saro_0799) (Vladimirova et al., 2016) are conserved around *N. aromaticivorans* DSM 12444 *nov1* (Saro_0802), which shows a 79% amino acid sequence identity with *lsdD* (Fig. S9). A recent biosensor study by Sun et al. showed that a DesR homolog, Saro_0803, binds to the *nov1* promoter region and represses the *nov1* transcription (Sun et al., 2020). Saro_0803 responded to stilbenes, including resveratrol, piceatannol, and pinosylvin. However, the response of Saro_0803 to vanillate and the response of Saro_0803 and DesR to lignostilbenes, such as DCA-S have not been examined (Araki et al., 2019; Sun et al., 2020). Further analysis of the effector molecules of Saro_0803 and DesR would provide new insights into the bacterial degradation system of stilbenoids and lignin-derived dimers degraded via lignostilbenes.

Purified LsdG showed comparable DCA-S conversion activity to LsdD (approx. 90%) (Fig. 2A). Besides, transcription levels of *lsdG* were 58% and 72% of those of *lsdD* in SYK-6 cells grown in Wx-SEMP and Wx-SEMP supplemented with vanillate, respectively (Fig. 3B). These results suggest that *lsdG* contribute to DCA-S conversion in SYK-6, but strangely enough, disruption of *lsdG* had little effect on DCA-S conversion activity, and Δ*lsdD* completely lost its activity (Fig. 4). It is difficult to explain these unexpected results, but one hypothesis is that it may be related to the fact that LSD produces homodimers and heterodimers. Kamoda et al. reported that $LsdA_{TMY}$ and $LsdB_{TMY}$ form homodimers (LSD-I

400 and LSD-III) and a heterodimer (LSD-II), whereas Lsdγ forms only a homodimer (LSD-IV)
401 in TMY1009 (Kamoda and Saburi, 1993; Kamoda et al., 1997). The DCA-S conversion
402 activity of LSD-III was 16.7-fold higher than that of LSD-I, and the activity of LSD-II toward
403 DCA-S was intermediate between LSD-I and LSD-III (Kamoda and Saburi, 1993). LSD
404 activity in SYK-6 is expected to depend not only on the amounts of each LSD gene product
405 but also on the state of the homodimer and heterodimer formation in vivo. Because LsdH,
406 LsdG, and LsdD are nearly equivalent to $LsdA_{TMY}$, $LsdB_{TMY}$, and Lsdγ at the amino acid
407 sequence levels, it is likely that these SYK-6 enzymes also form similar dimers in vivo as
408 well as LSD I, II, III, and IV of TMY1009. Therefore, LsdG-LsdH heterodimer's DCA-S
409 conversion activity is expected to be lower than LigG homodimer. Such heterodimer
410 formation between LSDs may result in the low abundance of LigG homodimer in the cells,
411 thus reducing the contribution of LigG to DCA-S conversion in vivo. However, this
412 hypothesis needs to be tested in the future by examining the abundance of LSD homodimers
413 and heterodimers in SYK-6 cells.

Acknowledgments

This work was supported in part by a grant from the Development of Preparatory Basic Bioenergy Technology grant from The New Energy and Industrial Technology Development Organization (NEDO) of Japan and the Advanced Low Carbon Technology Research and Development Program grant from The Japan Science and Technology Agency (Grant No. JPMJAL1107).

References

Araki, T., Tanatani, K., Kamimura, N., Otsuka, Y., Yamaguchi, M., Nakamura, M., Masai, E., 2020. The syringate *O*-demethylase gene of *Sphingobium* sp. strain SYK-6 is regulated by DesX, while other vanillate and syringate catabolism genes are regulated by DesR. Appl. Environ. Microbiol. 86 (22), e01712-20. https://doi.org/10.1128/AEM.01712-20

Araki, T., Umeda, S., Kamimura, N., Kasai, D., Kumano, S., Abe, T., Kawazu, C., Otsuka, Y., Nakamura, M., Katayama, Y., Fukuda, M., Masai, E., 2019. Regulation of vanillate and syringate catabolism by a MarR-type transcriptional regulator DesR in *Sphingobium* sp. SYK-6. Sci. Rep. 9 (1), 18036. https://doi.org/10.1038/s41598-019-54490-7

Becker, J., Wittmann, C., 2019. A field of dreams: Lignin valorization into chemicals, materials, fuels, and health-care products. Biotechnol. Adv. 37 (6), 107360. https://doi.org/10.1016/j.biotechadv.2019.02.016.

Beckham, G.T., Johnson, C.W., Karp, E.M., Salvachúa, D., Vardon, D.R., 2016. Opportunities and challenges in biological lignin valorization. Curr. Opin. Biotechnol. 42 40-53. https://doi.org/10.1016/j.copbio.2016.02.030

Bugg, T.D., Ahmad, M., Hardiman, E.M., Singh, R., 2011. The emerging role for bacteria in lignin degradation and bio-product formation. Curr. Opin. Biotechnol. 22 (3), 394-400. https://doi.org/10.1016/j.copbio.2010.10.009

Daruwalla, A., Kiser, P.D., 2020. Structural and mechanistic aspects of carotenoid cleavage dioxygenases (CCDs). Biochim. Biophys. Acta Mol. Cell Biol. Lipids 1865 (11), 158590. https://doi.org/10.1016/j.bbalip.2019.158590

Davin, L.B., Wang, H.B., Crowell, A.L., Bedgar, D.L., Martin, D.M., Sarkanen, S., Lewis, N.G., 1997. Stereoselective bimolecular phenoxy radical coupling by an auxiliary (dirigent) protein without an active center. Science 275 (5298), 362-366. https://doi.org/10.1126/science.275.5298.362

Floudas, D., Binder, M., Riley, R., Barry, K., Blanchette, R.A., Henrissat, B., Martínez, A.T., Otillar, R., Spatafora, J.W., Yadav, J.S., Aerts, A., Benoit, I., Boyd, A., Carlson, A., Copeland, A., Coutinho, P.M., de Vries, R.P., Ferreira, P., Findley, K., Foster, B., Gaskell, J., Glotzer, D., Górecki, P., Heitman, J., Hesse, C., Hori, C., Igarashi, K., Jurgens, J.A., Kallen, N., Kersten, P., Kohler, A., Kües, U., Kumar, T.K., Kuo, A., LaButti, K., Larrondo, L.F., Lindquist, E., Ling, A., Lombard, V., Lucas, S., Lundell, T., Martin, R., McLaughlin, D.J., Morgenstern, I., Morin, E., Murat, C., Nagy, L.G., Nolan, M., Ohm, R.A., Patyshakuliyeva, A., Rokas, A., Ruiz-Dueñas, F.J., Sabat, G., Salamov, A., Samejima, M., Schmutz, J., Slot, J.C., St John, F., Stenlid, J., Sun, H., Sun, S., Syed, K., Tsang, A., Wiebenga, A., Young, D., Pisabarro, A., Eastwood, D.C., Martin, F., Cullen, D.,

Grigoriev, I.V., Hibbett, D.S., 2012. The Paleozoic origin of enzymatic lignin decomposition reconstructed from 31 fungal genomes. Science 336 (6089), 1715-1719. https://doi.org/10.1126/science.1221748

Fujita, M., Mori, K., Hara, H., Hishiyama, S., Kamimura, N., Masai, E., 2019. A TonB-dependent receptor constitutes the outer membrane transport system for a lignin-derived aromatic compound. Commun. Biol. 2 432. https://doi.org/10.1038/s42003-019-0676-z

Fukuhara, Y., Inakazu, K., Kodama, N., Kamimura, N., Kasai, D., Katayama, Y., Fukuda, M., Masai, E., 2010. Characterization of the isophthalate degradation genes of *Comamonas* sp. strain E6. Appl. Environ. Microbiol. 76 (2), 519-527. https://doi.org/10.1128/AEM.01270-09

Habu, N., Komatsu, T., Samejima, M., Yoshimoto, T., 1989a. Metabolism of a diarylpropane type lignin model compound by *Pseudomonas* sp. TMY1009. Mokuzai Gakkaishi 35 348-355.

Habu, N., Samejima, M., Yoshimoto, T., 1988. Metabolic pathway of dehydrodiconiferyl alcohol by *Pseudomonas* sp. TMY1009. Mokuzai Gakkaishi 34 1026-1034.

Habu, N., Samejima, M., Yoshimoto, T., 1989b. A novel dioxygenase responsible for the Cα-Cβ cleavage of lignin model compounds from *Pseudomonas* sp. TMY1009. Mokuzai Gakkaishi 35 26-29.

Higuchi, Y., Aoki, S., Takenami, H., Kamimura, N., Takahashi, K., Hishiyama, S., Lancefield, C.S., Ojo, O.S., Katayama, Y., Westwood, N.J., Masai, E., 2018. Bacterial catabolism of β-hydroxypropiovanillone and β-hydroxypropiosyringone produced in the reductive cleavage of arylglycerol-β-aryl ether in lignin. Appl. Environ. Microbiol. 84 (7), e02670-17. https://doi.org/10.1128/AEM.02670-17

Higuchi, Y., Takahashi, K., Kamimura, N., Masai, E., 2017. Bacterial enzymes for the cleavage of lignin β-aryl ether bonds: properties and applications, In: Beckham, G.T. (Ed.), Lignin Valorization: Emerging Approaches. Royal Society of Chemistry, London, UK, pp. 226-251.

Johnson, M., Zaretskaya, I., Raytselis, Y., Merezhuk, Y., McGinnis, S., Madden, T.L., 2008. NCBI BLAST: a better web interface. Nucleic. Acids Res. 36 W5-9. https://doi.org/10.1093/nar/gkn201

Kaczmarczyk, A., Vorholt, J.A., Francez-Charlot, A., 2012. Markerless gene deletion system for sphingomonads. Appl. Environ. Microbiol. 78 (10), 3774-3777. https://doi.org/10.1128/Aem.07347-11

Kamimura, N., Goto, T., Takahashi, K., Kasai, D., Otsuka, Y., Nakamura, M., Katayama, Y., Fukuda, M., Masai, E., 2017a. A bacterial aromatic aldehyde dehydrogenase critical for the efficient catabolism of syringaldehyde. Sci. Rep. 7 44422. https://doi.org/10.1038/srep44422

Kamimura, N., Sakamoto, S., Mitsuda, N., Masai, E., Kajita, S., 2019. Advances in microbial lignin degradation and its applications. Curr. Opin. Biotechnol. 56 179-186. https://doi.org/10.1016/j.copbio.2018.11.011

Kamimura, N., Takahashi, K., Mori, K., Araki, T., Fujita, M., Higuchi, Y., Masai, E., 2017b. Bacterial catabolism of lignin-derived aromatics: New findings in a recent decade: Update on bacterial lignin catabolism. Environ. Microbiol. Rep. 9 (6), 679-705. https://doi.org/10.1111/1758-2229.12597

Kamoda, S., Habu, N., Samejima, M., 1989. Purification and some properties of lignostilbene-α,β-dioxygenase responsible for the Cα-Cβ cleavage of a diarylpropane type lignin model compound from *Pseudomonas* sp. TMY1009. Agric. Biol. Chem. 53 (10), 2757-2761. https://doi.org/10.1080/00021369.1989.10869724

Kamoda, S., Saburi, Y., 1993. Structural and enzymatical comparison of lignostilbene-α,β-dioxygenase isozymes, I, II, and III, from *Pseudomonas paucimobilis* TMY1009. Biosci. Biotechnol. Biochem. 57 (6), 931-934. https://doi.org/10.1271/bbb.57.931

Kamoda, S., Terada, T., Saburi, Y., 1997. Purification and some properties of lignostilbene-α,β-dioxygenase isozyme IV from *Pseudomonas paucimobilis* TMY1009. Biosci. Biotechnol. Biochem. 61 (9), 1575-1576. https://doi.org/10.1271/bbb.61.1575

Kamoda, S., Terada, T., Saburi, Y., 2005. Production of heterogeneous dimer lignostilbenedioxygenase II from *lsdA* and *lsdB* in *Escherichia coli* cells. Biosci. Biotechnol. Biochem. 69 (3), 635-637. https://doi.org/10.1271/bbb.69.635

Kuatsjah, E., Verstraete, M.M., Kobylarz, M.J., Liu, A.K.N., Murphy, M.E.P., Eltis, L.D., 2019. Identification of functionally important residues and structural features in a bacterial lignostilbene dioxygenase. J. Biol. Chem. 294 (35), 12911-12920. https://doi.org/10.1074/jbc.RA119.009428

Kumar, S., Stecher, G., Li, M., Knyaz, C., Tamura, K., 2018. MEGA X: Molecular evolutionary genetics analysis across computing platforms. Mol. Biol. Evol. 35 (6), 1547-1549. https://doi.org/10.1093/molbev/msy096

Lewis, N.G., Davin, L.B., Sarkanen, S., 1998. Lignin and lignan biosynthesis: distinctions and reconciliations, In: Lewis, N.G., Sarkanen, S. (Eds.), Lignin and Lignan Biosynthesis. ACS Publications, pp. 1-27.

Madeira, F., Park, Y.M., Lee, J., Buso, N., Gur, T., Madhusoodanan, N., Basutkar, P., Tivey, A.R.N., Potter, S.C., Finn, R.D., Lopez, R., 2019. The EMBL-EBI search and sequence analysis tools APIs in 2019. Nucleic. Acids Res. 47 (W1), W636-W641. https://doi.org/10.1093/nar/gkz268

Marasco, E.K., Schmidt-Dannert, C., 2008. Identification of bacterial carotenoid cleavage dioxygenase

507 homologues that cleave the interphenyl α,β double bond of stilbene derivatives via a monooxygenase reaction.
508 Chembiochem : a European journal of chemical biology 9 (9), 1450-1461.
509 https://doi.org/10.1002/cbic.200700724

510 Martínez, A., Camarero, S., Ruiz-Dueñas, F., Martínez, M., 2018. Biological lignin degradation, In: Beckham,
511 G.T. (Ed.), Lignin Valorization: Emerging Approaches. The Royal Society of Chemistry, London, UK, pp. 199-
512 225.

513 Martínez, A.T., Ruiz-Dueñas, F.J., Martínez, M.J., Del Río, J.C., Gutiérrez, A., 2009. Enzymatic delignification
514 of plant cell wall: from nature to mill. Curr. Opin. Biotechnol. 20 (3), 348-357.
515 https://doi.org/10.1016/j.copbio.2009.05.002

516 Masai, E., Katayama, Y., Fukuda, M., 2007. Genetic and biochemical investigations on bacterial catabolic
517 pathways for lignin-derived aromatic compounds. Biosci. Biotechnol. Biochem. 71 (1), 1-15.
518 https://doi.org/10.1271/bbb.60437

519 Mori, K., Kamimura, N., Masai, E., 2018. Identification of the protocatechuate transporter gene in *Sphingobium*
520 sp. strain SYK-6 and effects of overexpression on production of a value-added metabolite. Appl. Microbiol.
521 Biotechnol. 102 (11), 4807-4816. https://doi.org/10.1007/s00253-018-8988-3

522 Peng, X., Masai, E., Kasai, D., Miyauchi, K., Katayama, Y., Fukuda, M., 2005. A second 5-carboxyvanillate
523 decarboxylase gene, *ligW2*, is important for lignin-related biphenyl catabolism in *Sphingomonas paucimobilis*
524 SYK-6. Appl. Environ. Microbiol. 71 (9), 5014-5021. https://doi.org/10.1128/AEM.71.9.5014-5021.2005

525 Poliakov, E., Uppal, S., Rogozin, I.B., Gentleman, S., Redmond, T.M., 2020. Evolutionary aspects and
526 enzymology of metazoan carotenoid cleavage oxygenases. Biochim. Biophys. Acta Mol. Cell Biol. Lipids 1865
527 (11), 158665. https://doi.org/10.1016/j.bbalip.2020.158665

528 Ralph, J., Lapierre, C., Boerjan, W., 2019. Lignin structure and its engineering. Curr. Opin. Biotechnol. 56 240-
529 249. https://doi.org/10.1016/j.copbio.2019.02.019

530 Shinoda, E., Takahashi, K., Abe, N., Kamimura, N., Sonoki, T., Masai, E., 2019. Isolation of a novel platform
531 bacterium for lignin valorization and its application in glucose-free *cis*,*cis*-muconate production. J. Ind.
532 Microbiol. Biotechnol. 46 (8), 1071-1080. https://doi.org/10.1007/s10295-019-02190-6

533 Sievers, F., Wilm, A., Dineen, D., Gibson, T.J., Karplus, K., Li, W., Lopez, R., McWilliam, H., Remmert, M.,
534 Söding, J., Thompson, J.D., Higgins, D.G., 2011. Fast, scalable generation of high-quality protein multiple
535 sequence alignments using Clustal Omega. Mol. Syst. Biol. 7 (1), 539. https://doi.org/10.1038/msb.2011.75

Sonoki, T.i., Takahashi, K., Sugita, H., Hatamura, M., Azuma, Y., Sato, T., Suzuki, S., Kamimura, N., Masai, E., 2017. Glucose-free *cis*,*cis*-muconic acid production via new metabolic designs corresponding to the heterogeneity of lignin. ACS Sustain. Chem. Eng. 6 (1), 1256-1264. https://doi.org/10.1021/acssuschemeng.7b03597

Sun, H., Zhao, H., Ang, E.L., 2020. A new biosensor for stilbenes and a cannabinoid enabled by genome mining of a transcriptional regulator. ACS Synth. Biol. 9 (4), 698-705. https://doi.org/10.1021/acssynbio.9b00443

Takahashi, K., Hirose, Y., Kamimura, N., Hishiyama, S., Hara, H., Araki, T., Kasai, D., Kajita, S., Katayama, Y., Fukuda, M., Masai, E., 2015. Membrane-associated glucose-methanol-choline oxidoreductase family enzymes PhcC and PhcD are essential for enantioselective catabolism of dehydrodiconiferyl alcohol. Appl. Environ. Microbiol. 81 (23), 8022-8036. https://doi.org/10.1128/AEM.02391-15

Takahashi, K., Kamimura, N., Hishiyama, S., Hara, H., Kasai, D., Katayama, Y., Fukuda, M., Kajita, S., Masai, E., 2014. Characterization of the catabolic pathway for a phenylcoumaran-type lignin-derived biaryl in *Sphingobium* sp. strain SYK-6. Biodegradation 25 (5), 735-745. https://doi.org/10.1007/s10532-014-9695-0

Takahashi, K., Miyake, K., Hishiyama, S., Kamimura, N., Masai, E., 2018. Two novel decarboxylase genes play a key role in the stereospecific catabolism of dehydrodiconiferyl alcohol in *Sphingobium* sp. strain SYK-6. Environ. Microbiol. 20 (5), 1739-1750. https://doi.org/10.1111/1462-2920.14099

Vanholme, R., De Meester, B., Ralph, J., Boerjan, W., 2019. Lignin biosynthesis and its integration into metabolism. Curr. Opin. Biotechnol. 56 230-239. https://doi.org/10.1016/j.copbio.2019.02.018

Vanholme, R., Demedts, B., Morreel, K., Ralph, J., Boerjan, W., 2010. Lignin biosynthesis and structure. Plant Physiol. 153 (3), 895-905. https://doi.org/10.1104/pp.110.155119

Vladimirova, A., Patskovsky, Y., Fedorov, A.A., Bonanno, J.B., Fedorov, E.V., Toro, R., Hillerich, B., Seidel, R.D., Richards, N.G., Almo, S.C., Raushel, F.M., 2016. Substrate distortion and the catalytic reaction mechanism of 5-carboxyvanillate decarboxylase. J. Am. Chem. Soc. 138 (3), 826-836. https://doi.org/10.1021/jacs.5b08251

Supporting Information

LsdD has a Critical Role in the Dehydrodiconiferyl Alcohol Catabolism among Eight Lignostilbene α,β-dioxygenase Isozymes in *Sphingobium* sp. Strain SYK-6

Naofumi Kamimura[a], Yusaku Hirose[a], Ryuto Masuba[a], Ryo Kato[a], Kenji Takahashi[a], Yudai Higuchi[a], Shojiro Hishiyama[b], and Eiji Masai[a*]

[a]Department of Bioengineering, Nagaoka University of Technology, Nagaoka, Niigata 940-2188, Japan
[b]Forestry and Forest Products Research Institute, Tsukuba, Ibaraki 305-8687, Japan

[*]For correspondence. Eiji Masai, Department of Bioengineering, Nagaoka University of Technology, Nagaoka, Niigata 940-2188, Japan. E-mail emasai@vos.nagaokaut.ac.jp; Tel. +81 258479428; Fax +81 258479450

Contents

Supplementary tables: Tables S1–S4
Supplementary methods
Supplementary figures: Figs. S1–S9

Table S1. Strains and plasmids used in this study

Strain or plasmid	Relevant characteristic(s)[a]	Reference or source
Strains		
Sphingobium sp.		
SYK-6	Wild type; NBRC 103272/JCM 17495, Nal^r Sm^r	(Katayama et al., 1987)
SME112 (Δ*phcCD*)	SYK-6 derivative; *phcC-phcD*::*kan*; Nal^r Sm^r Km^r	(Takahashi et al., 2015)
SME260 (Δ*lsdA*)	SYK-6 derivative; deletion mutant of *lsdA*; Nal^r Sm^r	This study
SME261 (Δ*lsdD*)	SYK-6 derivative; deletion mutant of *lsdD*; Nal^r Sm^r	This study
SME264 (Δ*lsdG*)	SYK-6 derivative; deletion mutant of *lsdG*; Nal^r Sm^r	This study
Sphingobium japonicum		
UT26S	Type strain, NBRC 101211/JCM 17232, γ-hexachlorocyclohexane degradation	(Nagata et al., 2019)
Pseudomonas putida		
PpY1100	Nal^r	(Katayama et al., 1987)
E. coli		
NEB 10-beta	Δ(*ara-leu*) *7697 araD139 fhuA* Δ*lacX74 galK16 galE15 e14-* ϕ*80*d*lacZ*Δ*M15 recA1 relA1 endA1 nupG rpsL* (Sm^r) *rph spoT1* Δ(*mrr-hsdRMS-mcrBC*)	New England Biolabs
BL21(DE3)	F^- *ompT hsdSB*(r_B^- m_B^-) *gal dcm* (DE3); T7 RNA polymerase gene under control of the *lacUV5* promoter	(Studier and Moffatt, 1986)
HB101	*recA13 supE44 hsd20 ara-14 proA2 lacY1 galK2 rpsL20 xyl-5 mtl-1*	(Bolivar and Backman, 1979)
Plasmids		
pET-16b	Expression vector; T7 promoter, Ap^r	Novagen
pRK2013	Plasmid for parental mating; Tra^+ Mob^+ ColE1 replicon; Km^r	(Figurski and Helinski, 1979)
pAK405	Markerless gene deletion vector for Sphingomonads; Km^r	(Kaczmarczyk et al., 2012)
pBluescript II KS(+)	Cloning vector; Ap^r	(Short et al., 1988)
pQF	Expression vector for Sphingomonads; Q5 promoter, codon-optimized *cymR*; Tc^r	(Kaczmarczyk et al., 2013)
pJB864	RK2 broad-host-range expression vector; Ap^r Cb^r P_m *xylS*	(Blatny et al., 1997)
pET09440	pET-16b with a 1.5-kb PCR-amplicon carrying *lsdB*	This study
pET11300	pET-16b with a 1.5-kb PCR-amplicon carrying *lsdC*	This study
pET12580	pET-16b with a 1.5-kb PCR-amplicon carrying *lsdA*	This study
pET12860	pET-16b with a 1.5-kb PCR-amplicon carrying *lsdD*	This study
pET27300	pET-16b with a 1.5-kb PCR-amplicon carrying *lsdE*	This study
pET27970	pET-16b with a 1.5-kb PCR-amplicon carrying *lsdF*	This study
pET36640	pET-16b with a 1.5-kb PCR-amplicon carrying *lsdG*	This study
pET37540	pET-16b with a 1.5-kb PCR-amplicon carrying *lsdH*	This study
pBKS37540H	pBluescript II KS(+) with a 1.6-kb XbaI-BamHI fragment containing *lsdH*	This study
pAK12580	pAK405 with a 2.0-kb fragment containing up- and down-stream region of *lsdA*	This study
pAK12860	pAK405 with a 2.0-kb fragment containing up- and down-stream region of *lsdD*	This study
pAK36640	pAK405 with a 2.0-kb fragment containing up- and down-stream region of *lsdG*	This study
pQFlsdD	pQF with a 1.5-kb fragment carrying *lsdD*	This study
pQFlsdE	pQF with a 1.5-kb fragment carrying *lsdE*	This study
pJB37540	pJB864 with a 1.6-kb NotI-BamHI fragment carrying *lsdH*	This study

[a] Nal^r, Sm^r, Km^r, Ap^r, Tc^r, and Cb^r, resistance to nalidixic acid, streptomycin, kanamycin, ampicillin, tetracycline, and carbenicillin, respectively.

Table S2. Primers used in this study

Purpose, plasmids, and genes	Primers	Sequences (5′ to 3′)[a]
For construction of gene expression plasmids		
pET09440	09440_NdeI	GGAGAATTCATATGGTCGAACCAATCC
	09440_BamHI	AGGGGATCCCGGGATCAGGCCGCCG
pET11300	11300_NdeI	AGGAGATGCATATGACCACGTTTCC
	11300_XhoI	GTCCCTCGAGTTCCTTCCGCTCAGG
pET12580	12580_NdeI	TGGAGAGACATATGTCATTTCCCGC
	12580_BamHI	TCAGGATCCGCGAATTTGCTGCCTAGG
pET12860	12860_NdeI	AGGAGCAACATATGGCACATTTTCC
	12860_BamHI	TCGGGATCCATGCCCGGATCTCAGG
pET27300	27300_NdeI	GCCGGATCGAGAGTCATTCCCCATATGTCCC
	27300_XhoI	GCCGGGCGGGGTTTCTCGAGCGGCCTCACC
pET27970	27970_NdeI	AGGATCAGCATATGGCGAGTTTTCC
	27970_BamHI	AATGGATCCACGTGCCCTACGCCGC
pET36640	36640_NdeI	AGGAGAGCCATATGGCCCACTTCCC
	36640_BamHI	GCCGGATCCGGTGAGGCGGGCATCACG
pET37540	37540_NdeI	GGAGAGGACATATGGCCCATTTCCC
	37540_BamHI	ATGGGATCCTTTTTTGGCGAAGATGG
pQFlsdD	pQF12860_FW	CTAGTAGAGGAAGCTATGGGCCATCATCATCATCATCATAG CAGCGGCCATATGGCACATTTTCCCGACAC
	pQF12860_Rv	TCACTTCACCGGATCTCAGGCGGCGAGGCCGATCT
pQFlsdE	pQF27300_FW	CTAGTAGAGGAAGCTATGGGCCATCATCATCATCATCATAG CAGCGGCCATATGTCCCAAACATCAGACTT
	pQF27300_Rv	TCACTTCACCGGATCTCACCAGACATTGAGTTGCG
For qRT-PCR analysis		
16S rRNA	16S_qF	GCGCAGAACCTTACCAACGT
	16S_qR	AGCCATGCAGCACCTGTCA
lsdA	lsdA_pF	CAGCCGGGTGCTCTTCAA
	lsdA_pR	GTCTGCACATAGCGGATGTCA
lsdB	lsdB_pF	AAGGGCAGGTCCACATGCT
	lsdB_pR	ACCCACTTCACGACATAATCGA
lsdC	lsdC_pF	GCCTTCACCGGTTTCAACAC
	lsdC_pR	ACGTTGAGATCCTCGACATTGG
lsdD	lsdD_pF	TCGGCTCCTATCGCAATCC
	lsdD_pR	TTCGCGGTGGAGCGATAC
lsdE	lsdE_pF	GCCGTGGCGCAATACG
	lsdE_pR	GCGTCCGGCATTCACTTC
lsdF	lsdF_pF	TCCCGACACCATTCACTTCA
	lsdF_pR	TGCGCGTTCCATTCGAT
lsdG	lsdG_pF	CATCCCGATGCGCAATTC
	lsdG_pR	ATGCCATCCCCGTTGAAGA
lsdH	lsdH_pF	CCCCGGTTCGAGGATGAC
	lsdH_pR	GCGGAACAGGCTCACCAT
For construction of gene disruption plasmids		
pAK12580	Dis12580_TopF	CGGTACCCGGGGATCGATCGACGCGCATTGCCA
	Dis12580_TopR	ACATCTGCGGGAATCGTGC
	Dis12580_BotR	CGACTCTAGAGGATCACCCGCGAGAACTACATG
	Dis12580_BotF	GCACGATTCCCGCAGATGTTCTGGAATGCGGGCGATCT
pAK12860	Dis12860_TopF	CGGTACCCGGGGATCTCGGCAATGATGAGCGAGG
	Dis12860_TopR	TTCGGTCTGCACGGCAACTG
	Dis12860_BotR	CGACTCTAGAGGATCAAAGCACGACGCCCAGTT
	Dis12860_BotF	CAGTTGCCGTGCAGACCGAATCATGCACCAGGTTCGGA
pAK36640	Dis36640_TopF	CGGTACCCGGGGATCCTTCAACCCGTCCGTCACT
	Dis36640_TopR	GGATTTCCCCTTCGACTT
	Dis36640_BotR	CGACTCTAGAGGATCCGCACGAATTCGAAGGGCTG
	Dis36640_BotF	AAGTCGAAGGGGAAATCCCTGGACGCCCTGAACCTCAA
For confirmation of gene disruption		
lsdA	12580_sotogawa_F	CGCGACGCGGGGCATCGGGCCGGGC
	12580_sotogawa_R	GGCCTCGCCTTCGTGCCGCTGATCG
lsdD	12860_sotogawa_F	CGCGCGAGCGACGCGGCTGTCCGCG
	12860_sotogawa_R	CCAGACCGTCAGGGTCCACACATCG
lsdG	36640_sotogawa_F	GCCCGCCGAGCGTCTCGATGAGTCC
	Dis36640_BotR	CGACTCTAGAGGATCCGCACGAATTCGAAGGGCTG

[a]Underlines indicate the restriction enzyme site of NdeI, BamHI, or XhoI. The His-tag sequence is shown in red.

Table S3. Putative LSD genes in *Sphingobium* sp. SYK-6

Gene	Locus tag	Accession number	Identity (%)	Most similar Enzyme	Organism	Reference
lsdA	SLG_12580	BAK65933.1	54.6	NOV2 (ABD27245.1)	*Novosphingobium aromaticivorans* DSM 12444	(Marasco and Schmidt-Dannert, 2008)
lsdB	SLG_09440	BAK65619.1	39.6	isoeugenol monooxygenase (ACP17973.1)	*Pseudomonas nitroreducens* Jin1	(Ryu et al., 2013)
lsdC	SLG_11300	BAK65805.1	62.3	NOV1 (ABD25247.1)	*Novosphingobium aromaticivorans* DSM 12444	(Marasco and Schmidt-Dannert, 2008)
lsdD	SLG_12860	BAK65961.1	79.1	NOV1 (ABD25247.1)	*Novosphingobium aromaticivorans* DSM 12444	(Marasco and Schmidt-Dannert, 2008)
lsdE	SLG_27300	BAK67405.1	41.4	isoeugenol monooxygenase (AON53704.1)	*Herbaspirillum seropedicae* AU14040	(Han et al., 2019)
lsdF	SLG_27970	BAK67472.1	53.9	NOV2 (ABD27245.1)	*Novosphingobium aromaticivorans* DSM 12444	(Marasco and Schmidt-Dannert, 2008)
lsdG	SLG_36640	BAK68339.1	98.0	Lsdβ (Q52008.1)	*Sphingomonas paucimobilis* TMY1009	(Kamoda and Saburi, 1995)
lsdH	SLG_37540	BAK68429.1	98.6	Lsdα (Q53353.1)	*Sphingomonas paucimobilis* TMY1009	(Kamoda and Saburi, 1993)

Table S4. Induction profiles of *lsdA–lsdH* and DCA catabolism genes in SYK-6

Gene	DCA[a]		vanillate[a]		protocatechuate[a]	
	Ratio	*P*-value	Ratio	*P*-value	Ratio	*P*-value
lsdA	1.81	0.013	**2.27**	0.001	1.48	0.048
lsdB	1.20	0.000	1.04	0.606	1.40	0.175
lsdC	0.90	0.063	1.12	0.104	0.92	0.206
lsdD	**4.20**	0.000	**4.28**	0.002	1.34	0.023
lsdE	0.85	0.026	0.78	0.012	1.06	0.061
lsdF	1.18	0.032	0.88	0.013	1.59	0.213
lsdG	1.67	0.050	1.90	0.071	1.22	0.236
lsdH	1.31	0.097	**4.81**	0.036	1.34	0.105
phcC	**2.30**	0.081	1.16	0.016	0.81	0.493
phcD	**2.21**	0.013	0.66	0.006	0.83	0.064
phcF	**6.13**	0.003	1.03	0.670	1.18	0.329
phcG	**3.45**	0.018	0.80	0.058	0.83	0.188

[a]Data were retrieved from NCBI BioProject database (accession number, PRJNA555998). Transcription profiles were determined by DNA microarray analysis using total RNA extracted from SYK-6 cells grown in Wx-SEMP and Wx-SEMP supplemented with 2 mM DCA, 5 mM vanillate, or 5 mM protocatechuate (Fujita et al., 2019). The expression of each gene in the cells grown in Wx-SEMP plus 2 mM DCA, 5 mM vanillate, or 5 mM protocatechuate was compared with that of cells grown in Wx-SEMP using an in silico analysis performed using the loess method. Average normalized expression ratios (treatment/control) were calculated for each gene and tested for any significant variation between treatments (one-way ANOVA with Dunnett's multiple comparisons post-test). Each value was obtained from n = 3 independent experiments.

Supplementary methods

Preparations of HMPPD-S

Chemical synthesis of HMPPD-S

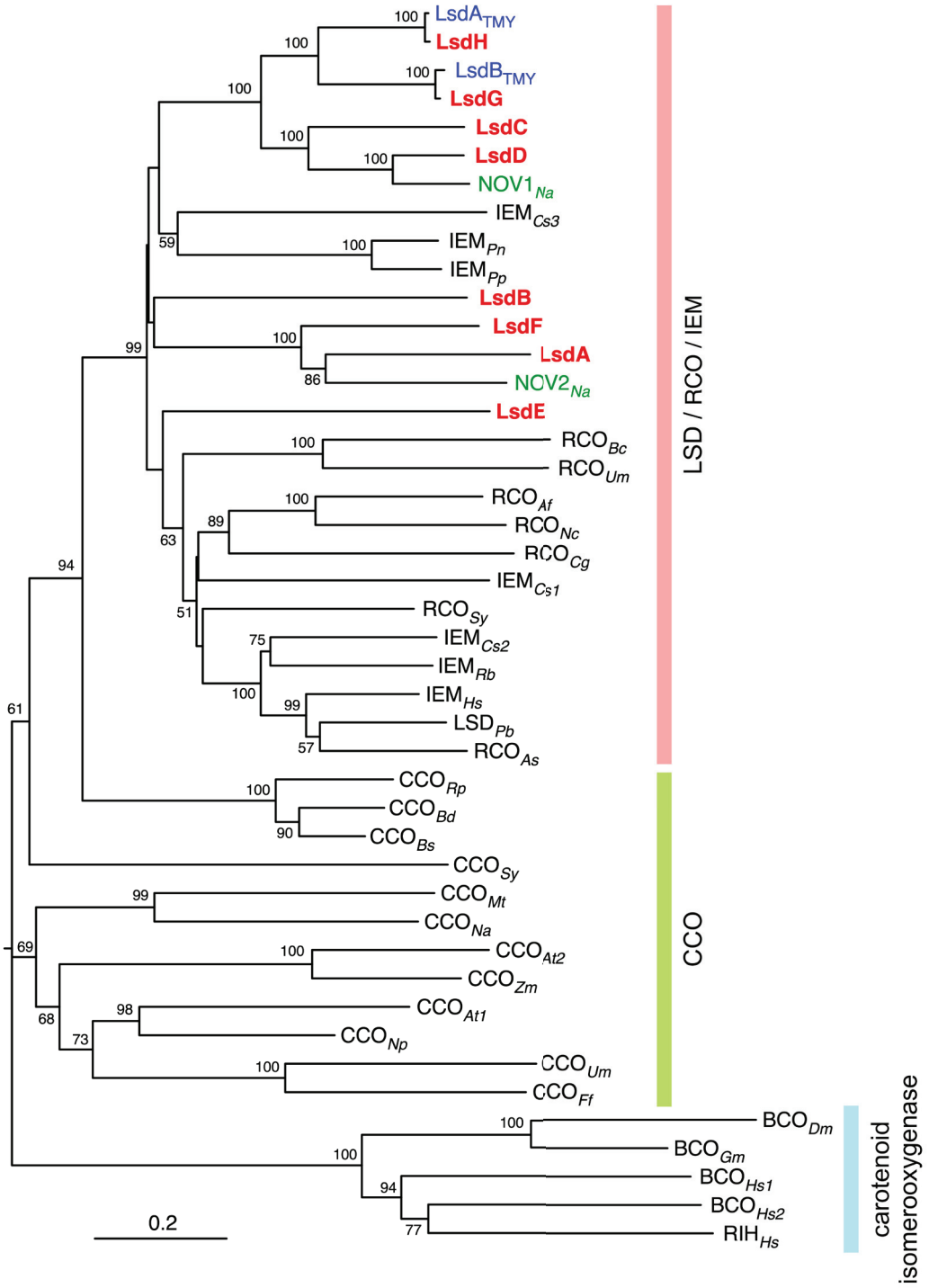

Fig. S1. Phylogenetic tree of LsdA–LsdH and previously characterized LSDs, resveratrol cleavage oxygenases (RCOs), isoeugenol monooxygenases (IEMs), carotenoid cleavage oxygenases (CCOs), and carotenoid isomerooxygenases.

The phylogenetic tree was constructed by neighbor-joining using 1,000 bootstrap replicates. Bootstrap values are indicated at the nodes, and the scale corresponds to 0.2 amino acid substitutions per position. LSD of SYK-6, *Sphingomonas paucimobilis* TMY 1009, and *Novosphingobium aromaticivorans* DSM 12444 are shown in bold red, blue, green, respectively. Enzymes: LsdA, LSD of *Sphingobium* sp. SYK-6 (BAK65933.1); LsdB, putative oxygenase of SYK-6 (BAK65619.1); LsdC, putative dioxygenase of SYK-6 (BAK65805.1); LsdD, hypothetical protein of SYK-6 (BAK65961.1); LsdE, putative dioxygenase of SYK-6 (BAK67405.1); LsdF, putative dioxygenase of SYK-6 (BAK67472.1); LsdG, putative dioxygenase of SYK-6 (BAK68339.1); LsdH, putative

dioxygenase of SYK-6 (BAK68429.1); $LsdA_{TMY}$, subunit of LSD I and II of *S. paucimobilis* TMY 1009 (AAC60447); $LsdB_{TMY}$, subunit of LSD II and III of *S. paucimobilis* TMY 1009 (AAB35856.2); $NOV1_{Na}$, LSD of *N. aromaticivorans* DSM 12444 (ABD25247.1); $NOV2_{Na}$, LSD of *N. aromaticivorans* DSM 12444 (ABD27245.1); LSD_{Pb}, LSD of *Pseudomonas brassicacearum* DF41 (AHL33370.1); RCO_{Af}, RCO of *Aspergillus fumigatus* Af293 (EAL84269.2); RCO_{As}, RCO of *Acinetobacter* sp. JS678 (AVI04967.1); RCO_{Bc}, RCO of *Botrytis cinerea* B05.10 (ATZ50468.1); RCO_{Cg}, RCO of *Chaetomium globosum* CBS 148.51 (EAQ91995.1); RCO_{Nc}, RCO of *Neurospora crassa* OR74A (EAA32528.1); RCO_{Um}, RCO of *Ustilago maydis* 521 (KIS70010.1); RCO_{Sy}, RCO of *Sphingobium yanoikuyae* JS1018 (ARQ83690.1); IEM_{Cs1}, IEM of *Caulobacter segnis* ATCC 21756 (ADG10197.1); IEM_{Cs2}, IEM of *C. segnis* ATCC 21756 (ADG10219.1); IEM_{Cs3}, IEM of *C. segnis* ATCC 21756 (ADG10224.1); IEM_{Hs}, IEM of *Herbaspirillum seropedicae* AU14040 (AON53704.1); IEM_{Pn}, IEM of *Pseudomonas nitroreducens* Jin1 (ACP17973.1); IEM_{Pp}, IEM of *Pseudomonas putida* IE27 (BAF62888.1); IEM_{Rb}, IEM of *Rhodobacteraceae bacterium* GWE1_64_9 (OHC44943.1); CCO_{At1}, carotenoid 9,10(9',10')-cleavage dioxygenase of *Arabidopsis thaliana* (CAA06712.1); CCO_{At2}, 9-*cis*-epoxycarotenoid dioxygenase NCED2 of *A. thaliana* (CAA16715.1); CCO_{Bd}, farnesol oxygenase of *Bradyrhizobium diazoefficiens* USDA 110 (AND90949.1); CCO_{Bs}, farnesol oxygenase of *Bradyrhizobium* sp. BTAi1 (ABQ37440.1); CCO_{Ff}, carotenoid oxygenase of *Fusarium fujikuroi* IMI58289 (CAH70723.1); CCO_{Mt}, CCO of *Mycobacterium tuberculosis* ATCC 25618 (CCP43397.1); CCO_{Na}, CCO of *N. aromaticivorans* DSM 12444 (ABP64440.1); CCO_{Np}, CCO of *Nostoc punctiforme* PCC 73102 (ACC81402.1); CCO_{Rp}, CCO of *Rhodopseudomonas palustris* CGA009 (CAE26651.1); CCO_{Sy2}, carotenoid cleavage oxygenase of *S. yanoikuyae* JS1018 (ARQ83691.1); CCO_{Um}, CCO of *U. maydis* 521 (KIS71050.1); CCO_{Zm}, 9-*cis*-epoxycarotenoid dioxygenase of *Zea mays* (AAB62181.2); BCO_{Dm}, carotenoid isomerooxygenase of *Drosophila melanogaster* (CAB93141.1); BCO_{Gm}, carotenoid isomerooxygenase of *Galleria mellonella* (CAO85888.1); BCO_{Hs1}, β, β-carotene 15,15'-dioxygenase of *Homo sapiens* (AAG15380.1); BCO_{Hs2}, β, β-carotene 9',10'-oxygenase of *H. sapiens* (AAK69433.1); RIH_{Hs}, retinoid isomerohydrolase of *H. sapiens* (AAA99012.1).

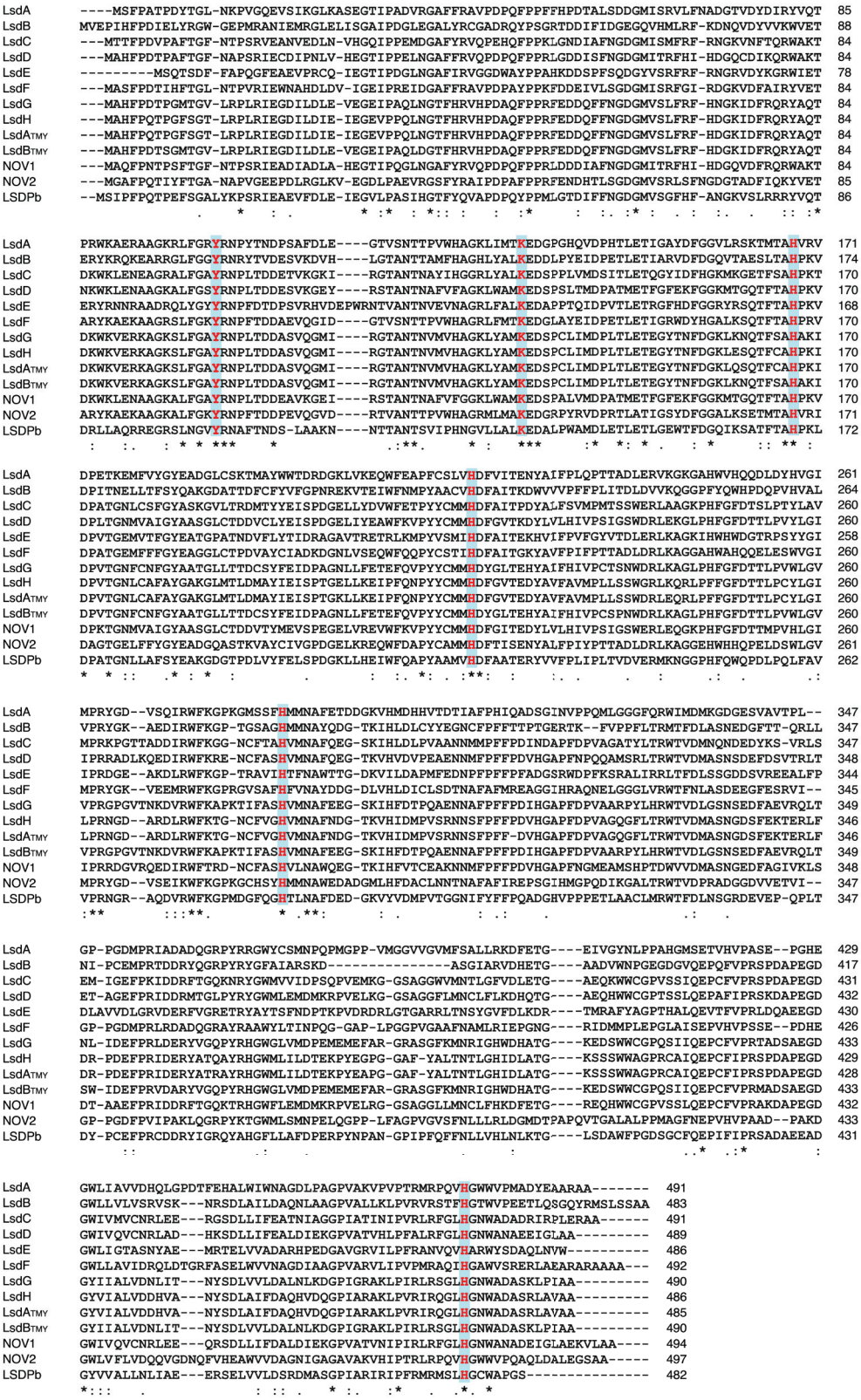

Fig. S2. Amino acid sequence alignment of LsdA–LsdH with bacterial LSDs.

Catalytically important amino acids, including His167$_{NOV1}$, His218$_{NOV1}$, His284$_{NOV1}$, His476$_{NOV1}$, Tyr101$_{NOV1}$, and Lys135$_{NOV1}$, are shown in red letters on a light-blue background.

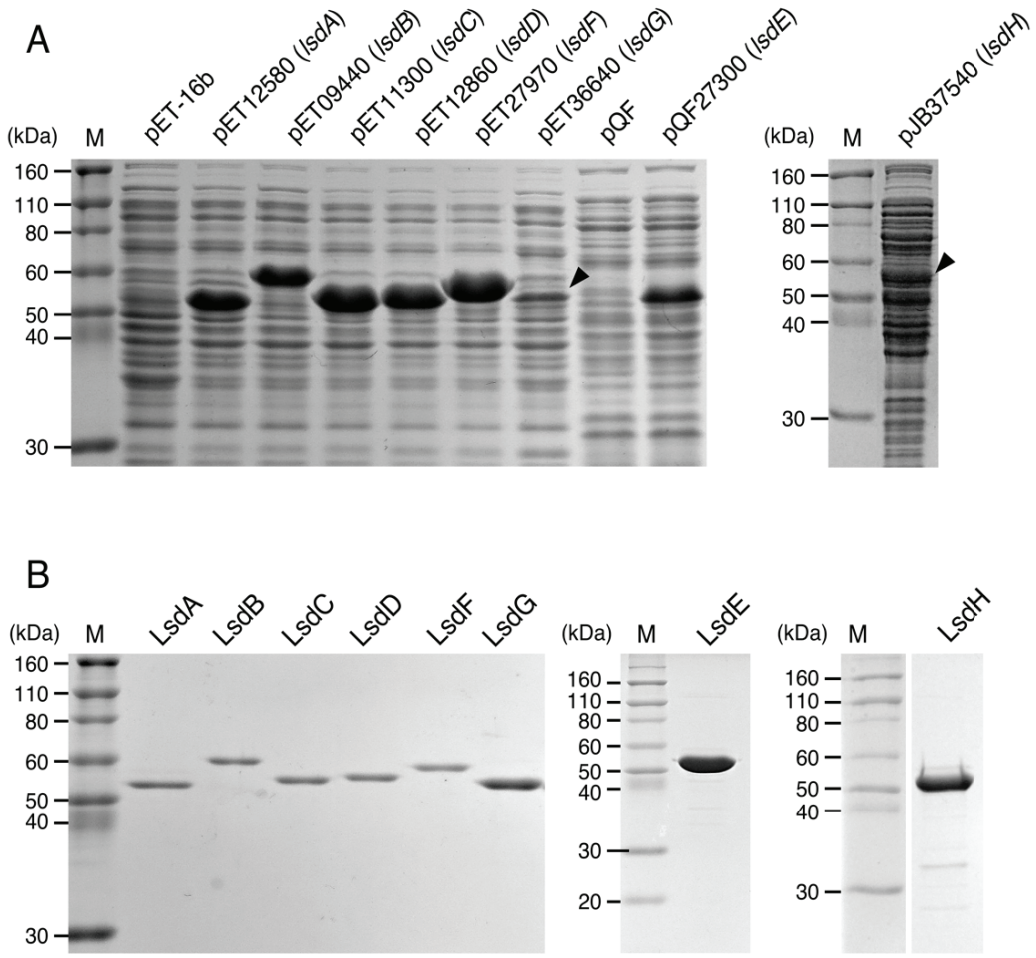

Fig. S3. Expression of *lsd* genes and purification of LsdA–LsdH.

(A) Expression of *lsd* genes in heterologous hosts. Cell extracts (10 μg protein/lane) of *E. coli* BL21(DE3) harboring pET-16b or pET-16b carrying *lsdA*, *lsdB*, *lsdC*, *lsdD*, *lsdF*, or *lsdG*, *Sphingobium japonicum* UT26S harboring pQF or pQF carrying *lsdE* (pQF27300), and *Pseudomonas putida* PpY1100 harboring pJB864 carrying *lsdH* (pJB37540) were separated by SDS-12% polyacrylamide gels and stained with Coomassie Brilliant Blue. **(B)** Purification of LsdA–LsdH. Each *lsd* gene product was purified by Ni affinity chromatography, and resultant purified proteins (LsdA, LsdB, LsdC, LsdD, LsdF, and LsdG, 1.0 μg protein/lane; LsdE and LsdG, 10 μg protein/lane) were separated by SDS-12% polyacrylamide gels and stained with Coomassie Brilliant Blue. M, molecular mass markers. The predicted molecular masses of His-tag-fused gene products of *lsdA*, *lsdB*, *lsdC*, *lsdD*, *lsdE*, *lsdF*, *lsdG*, and *lsdH* are 56,954, 57,069, 57,491, 57,434, 58,024, 56,746, 57,655, and 56,954 Da, respectively.

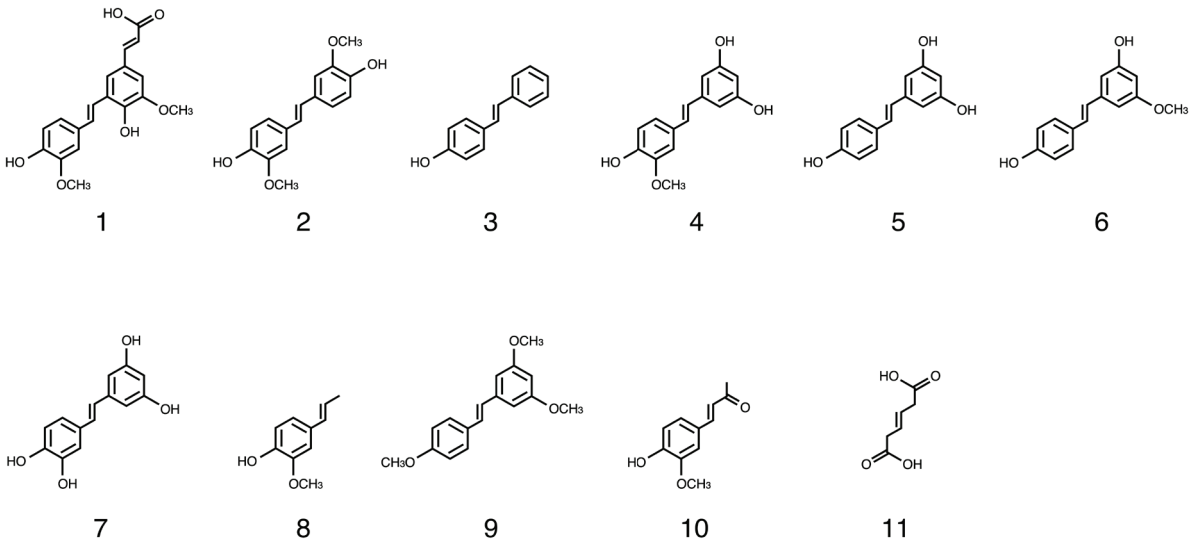

Fig. S4. Chemical structure of substrates used to determine the substrate range of LsdA–LsdH.
Compounds: 1, DCA-S; 2, HMPPD-S; 3, 4-hydroxystilbene; 4, isorhapontigenin; 5, resveratrol; 6, pinostilbene; 7, piceatannol; 8, isoeugenol; 9, 3,4',5-trimethoxy-stilbene; 10, dehydrozingerone; 11, 3-hexenedioate.

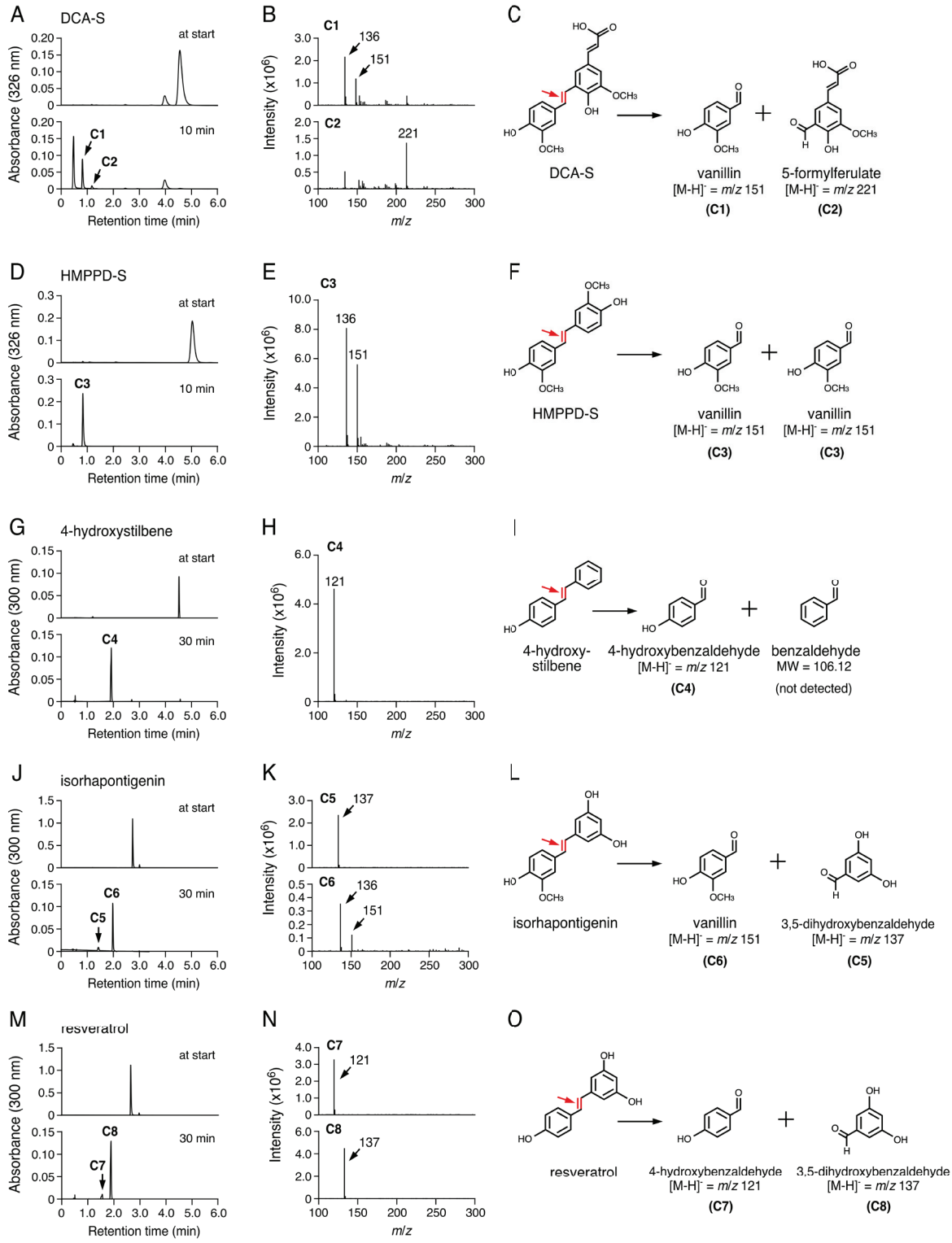

Fig. S5. HPLC–MS analysis of the conversion of each substrate by LsdD and conversion of HMPPD-S by LsdA–H.

(A–X) LsdD (20 μg of protein ml^{-1}) was incubated with 100 μM DCA-S, HMPPD-S, 4-hydroxystilbene, isorhapontigenin, resveratrol, pinostilbene, piceatannol, and isoeugenol for 10 min (DCA-S and HMPPD-S) or 30 min (other substrates) at 30°C. Reaction samples were analyzed by HPLC–MS. **(A, D, G, J, M, P, S, and V)** HPLC chromatograms at the start and after the reaction. C1–C13 are reaction products. The retention times for C11 and C12 were the same. Benzaldehyde and acetaldehyde were not detected. **(B, E, H, K, N, Q, T, and W)** The electrospray ionization (ESI)–MS spectra of C1–C13 (negative-ion mode) are shown. **(C, F, I, L, O, R, U,**

and X) Reaction scheme of each substrate conversion by LSD. **(Y)** Conversion of HMPPD-S by LsdA, LsdB, LsdC, LsdE, LsdF, LsdG, and LsdH. Purified enzymes (20 μg of protein ml^{-1}) were incubated with 100 μM HMPPD-S for 10 min at 30°C. Reaction samples were analyzed by HPLC. DCA-S and HMPPD-S were detected at 326 nm, and other compounds were detected at 300 nm. Retention times: DCA-S, 4.3 min; HMPPD-S, 5.1 min; 4-hydroxystilbene, 4.5 min; isorhapontigenin, 2.8 min; resveratrol, 2.8 min; pinostilbene, 3.6 min; piceatannol, 2.2 min; and isoeugenol, 3.8 min.

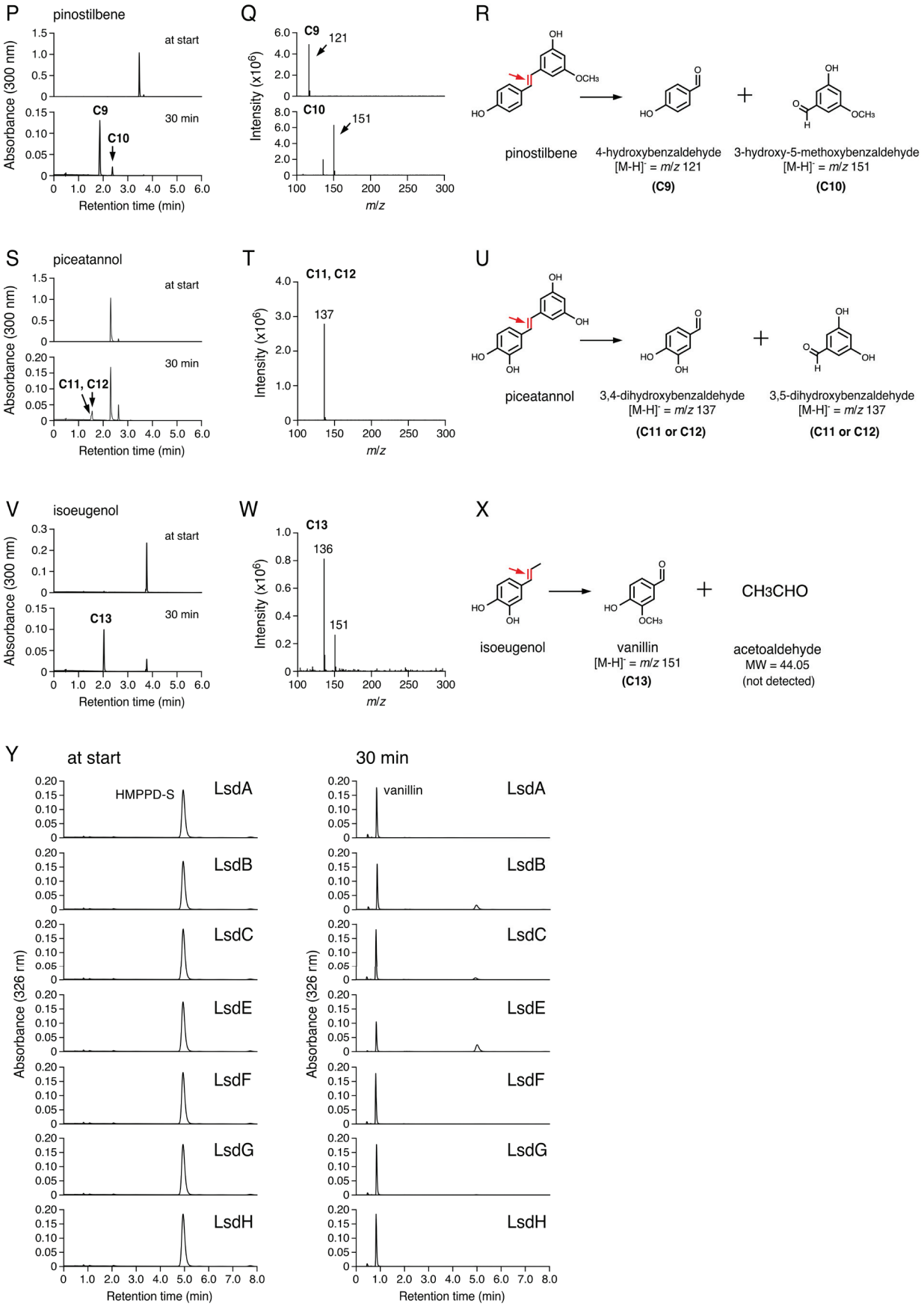

Fig. S5–*Continued*.

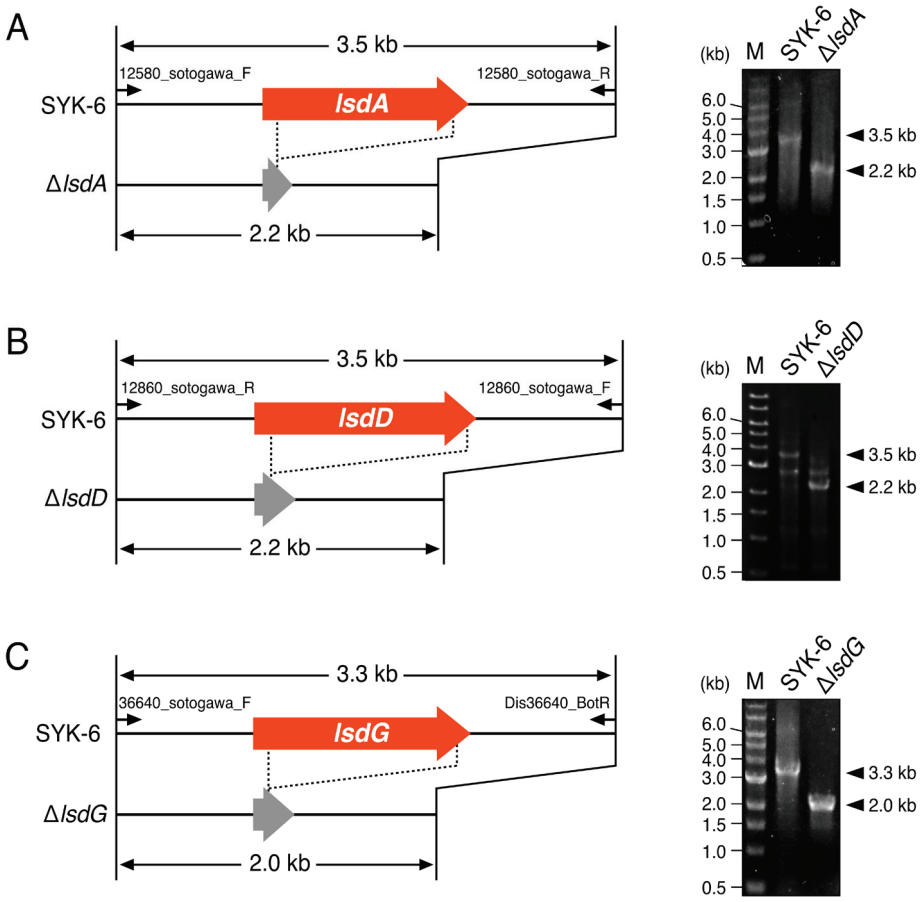

Fig. S6. Disruption of *lsdA*, *lsdD*, and *lsdG* in *Sphingobium* sp. SYK-6.
Schematic representations and colony PCR analyses of the disruption of *lsdA* (A), *lsdD* (B), and *lsdG* (C) in SYK-6. The primer pairs used for colony PCR analyses were indicated by one-way arrows and their sequences are shown in Table S2. M, molecular size markers.

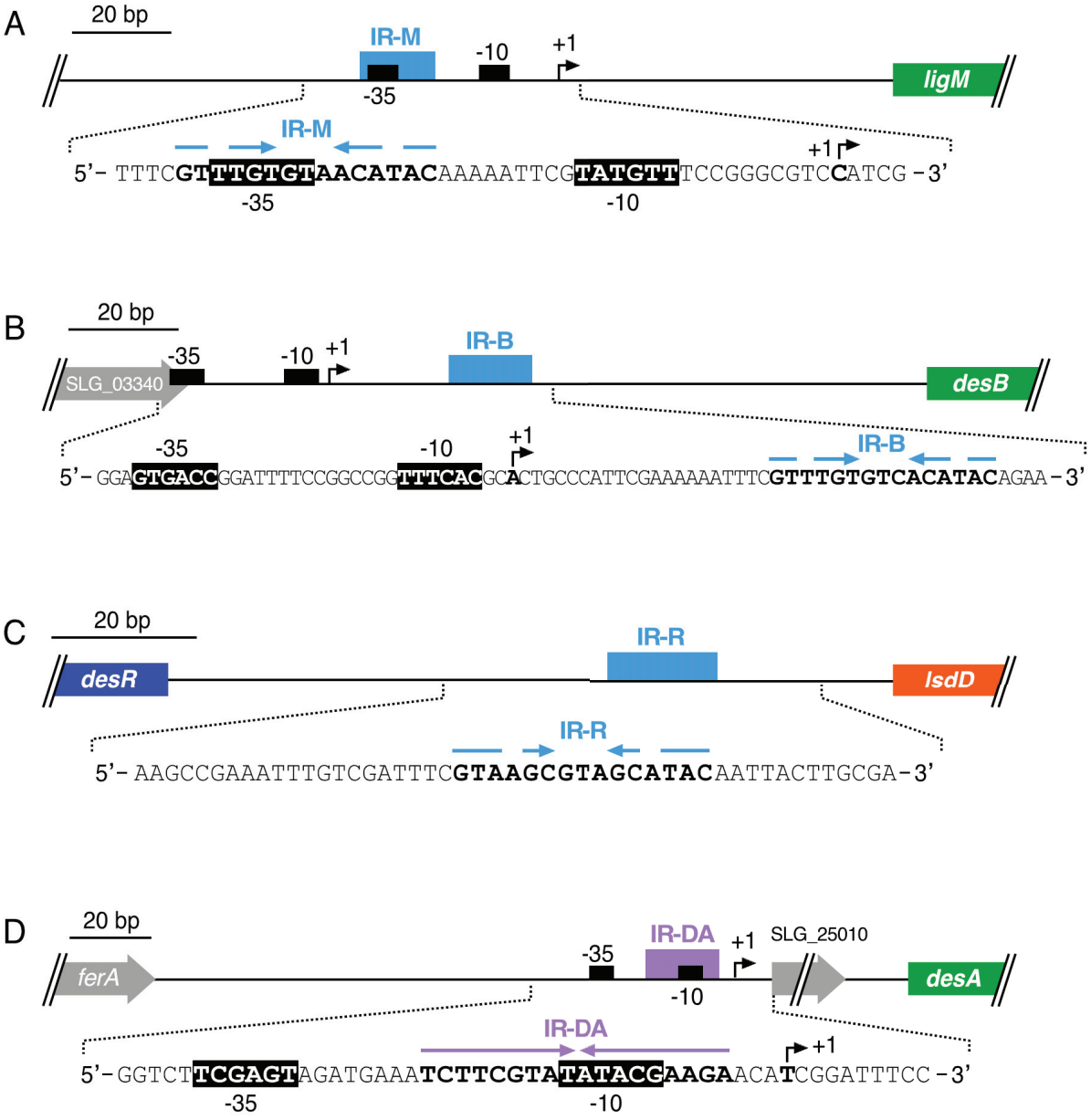

Fig. S7. Binding sites of DesR and DesX.

(A–C) DesR-binding sites located upstream of *ligM* (IR-M; A), upstream of *desB* (IR-B; B), and in the intergenic region of *desR* and *lsdD* (IR-R; C) are shown. **(D)** DesX binding site located upstream of *desA* (IR-DA) is displayed. The IR sequences are shown by convergent arrows. Transcription initiation sites are shown by bent arrows (+1). Putative –35 and –10 regions are indicated on black backgrounds.

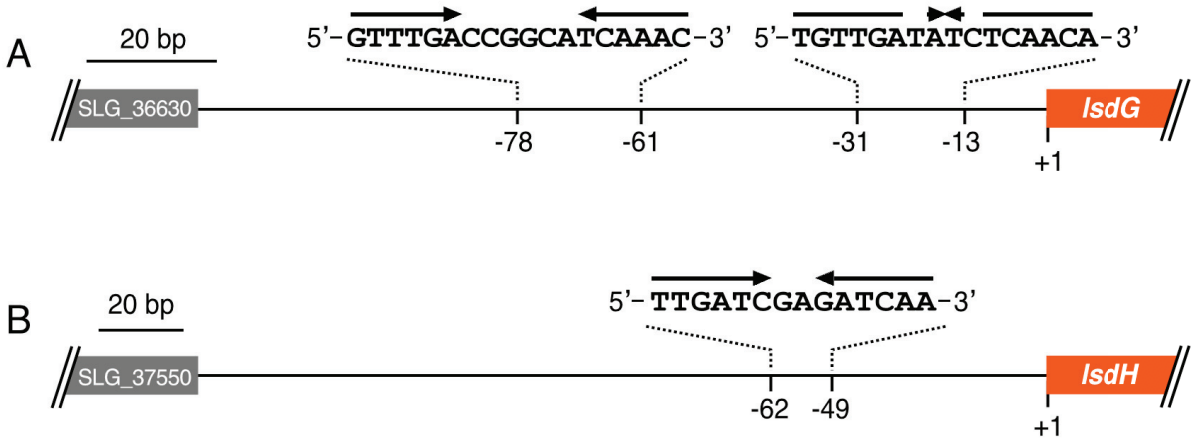

Fig. S8. Incomplete inverted repeat sequences found upstream of *lsdG* (A) and *lsdH* (B).
The IR sequences from the start codons (+1) of *lsdG* and *lsdH* are shown by convergent arrows.

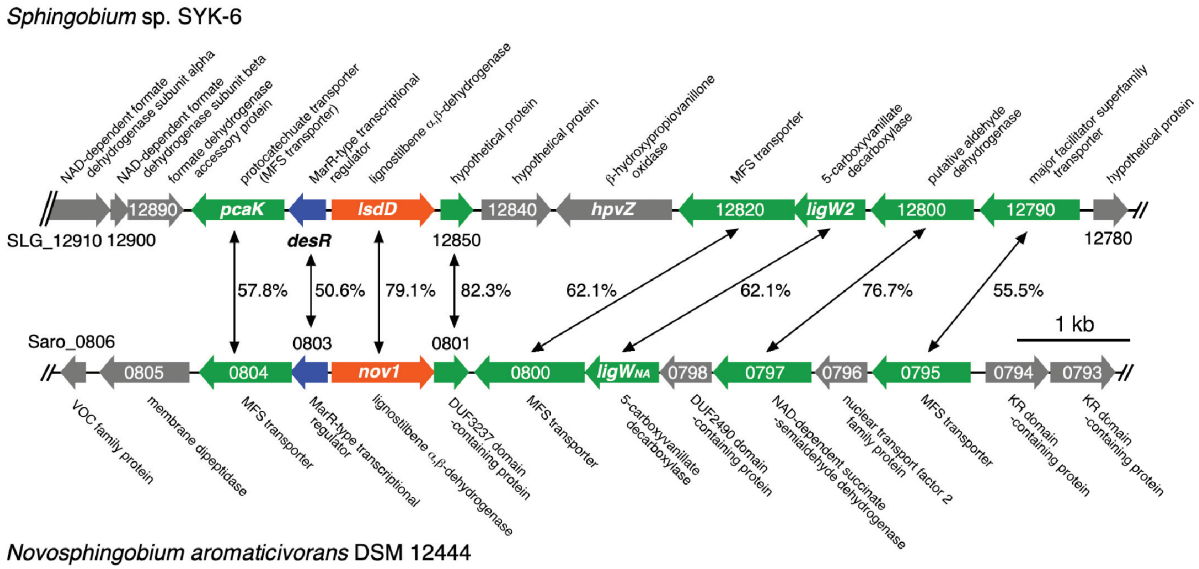

Fig. S9. Comparison of the gene organization around *lsdD* between *Sphingobium* sp. SYK-6 and *N. aromaticivorans* DSM 12444.

The amino acid sequence identities between the genes indicated by the double-headed arrows are shown.

References

Blatny, J.M., Brautaset, T., Winther-Larsen, H.C., Karunakaran, P., Valla, S., 1997. Improved broad-host-range RK2 vectors useful for high and low regulated gene expression levels in Gram-negative bacteria. Plasmid 38 (1), 35-51. https://doi.org/10.1006/plas.1997.1294

Bolivar, F., Backman, K., 1979. Plasmids of *Escherichia coli* as cloning vectors. Methods Enzymol. 68 245-267. https://doi.org/10.1016/0076-6879(79)68018-7

Figurski, D., Helinski, D., 1979. Replication of an origin-containing derivative of plasmid RK2 dependent on a plasmid function provided in trans. Proc. Natl. Acad. Sci. U S A 76 (4), 1648-1652.

Fujita, M., Mori, K., Hara, H., Hishiyama, S., Kamimura, N., Masai, E., 2019. A TonB-dependent receptor constitutes the outer membrane transport system for a lignin-derived aromatic compound. Commun. Biol. 2 432. https://doi.org/10.1038/s42003-019-0676-z

Han, Z., Long, L., Ding, S., 2019. Expression and characterization of carotenoid cleavage oxygenases from *Herbaspirillum seropedicae* and *Rhodobacteraceae bacterium* capable of biotransforming isoeugenol and 4-vinylguaiacol to vanillin. Front. Microbiol. 10 1869. https://doi.org/10.3389/fmicb.2019.01869

Kaczmarczyk, A., Vorholt, J.A., Francez-Charlot, A., 2012. Markerless gene deletion system for sphingomonads. Appl. Environ. Microbiol. 78 (10), 3774-3777. https://doi.org/10.1128/Aem.07347-11

Kaczmarczyk, A., Vorholt, J.A., Francez-Charlot, A., 2013. Cumate-inducible gene expression system for sphingomonads and other Alphaproteobacteria. Appl. Environ. Microbiol. 79 (21), 6795-802. https://doi.org/10.1128/AEM.02296-13

Kamoda, S., Saburi, Y., 1993. Cloning, expression, and sequence analysis of a lignostilbene-α,β-dioxygenase gene from *Pseudomonas paucimobilis* TMY1009. Biosci. Biotechnol. Biochem. 57 (6), 926-930. https://doi.org/10.1271/bbb.57.926

Kamoda, S., Saburi, Y., 1995. Cloning of a lignostilbene-α,β-dioxygenase isozyme gene from *Pseudomonas paucimobilis* TMY1009. Biosci. Biotechnol. Biochem. 59 (10), 1866-1868. https://doi.org/10.1271/bbb.59.1866

Katayama, Y., Nishikawa, S., Nakamura, M., Yano, K., Yamasaki, M., Morohoshi, N., Haraguchi, T., 1987. Cloning and expression of *Pseudomonas paucimobilis* SYK-6 genes involved in the degradation of vanillate and protocatechuate in *Pseudomonas putida*. Mokuzai Gakkaishi 33 77-79.

Marasco, E.K., Schmidt-Dannert, C., 2008. Identification of bacterial carotenoid cleavage dioxygenase homologues that cleave the interphenyl α,β double bond of stilbene derivatives via a monooxygenase reaction. Chembiochem : a European journal of chemical biology 9 (9), 1450-1461. https://doi.org/10.1002/cbic.200700724

Nagata, Y., Kato, H., Ohtsubo, Y., Tsuda, M., 2019. Lessons from the genomes of lindane-degrading

sphingomonads. Environmental Microbiology Reports 11 (5), 630-644. https://doi.org/10.1111/1758-2229.12762

Ryu, J.Y., Seo, J., Park, S., Ahn, J.H., Chong, Y., Sadowsky, M.J., Hur, H.G., 2013. Characterization of an isoeugenol monooxygenase (Iem) from *Pseudomonas nitroreducens* Jin1 that transforms isoeugenol to vanillin. Biosci. Biotechnol. Biochem. 77 (2), 289-294. https://doi.org/10.1271/bbb.120715

Short, J.M., Fernandez, J.M., Sorge, J.A., Huse, W.D., 1988. λ ZAP: a bacteriophage λ expression vector with *in vivo* excision properties. Nucleic. Acids Res. 16 (15), 7583-7600.

Studier, F.W., Moffatt, B.A., 1986. Use of bacteriophage T7 RNA polymerase to direct selective high-level expression of cloned genes. J. Mol. Biol. 189 (1), 113-130. https://doi.org/10.1016/0022-2836(86)90385-2

Takahashi, K., Hirose, Y., Kamimura, N., Hishiyama, S., Hara, H., Araki, T., Kasai, D., Kajita, S., Katayama, Y., Fukuda, M., Masai, E., 2015. Membrane-associated glucose-methanol-choline oxidoreductase family enzymes PhcC and PhcD are essential for enantioselective catabolism of dehydrodiconiferyl alcohol. Appl. Environ. Microbiol. 81 (23), 8022-8036. https://doi.org/10.1128/AEM.02391-15